SHARP-INTERFACE APPROACH FOR SIMULATING SOLID-STATE DEWETTING IN THREE DIMENSIONS

WEI JIANG*, QUAN ZHAO†, AND WEIZHU BAO‡

Abstract. The problem of simulating solid-state dewetting of thin films in three dimensions (3D) by using a sharp-interface approach is considered in this paper. Based on the thermodynamic variation, a speed method is used for calculating the first variation to the total surface energy functional. The speed method shares more advantages than the traditional use of parameterized curves (or surfaces), e.g., it is more intrinsic and its variational structure (related with Cahn-Hoffman $\boldsymbol{\xi}$-vector) is clearer and more direct. By making use of the first variation, necessary conditions for the equilibrium shape of the solid-state dewetting problem is given, and a kinetic sharp-interface model which includes the surface energy anisotropy is also proposed. This sharp-interface model describes the interface evolution in 3D which occurs through surface diffusion and contact line migration. By solving the proposed model, we perform lots of numerical simulations to investigate the evolution of patterned films, e.g., the evolution of a short cuboid and pinch-off of a long cuboid. Numerical simulations in 3D demonstrate the accuracy and efficacy of the sharp-interface approach to capture many of the complexities observed in solid-state dewetting experiments.

Key words. Solid-state dewetting, surface diffusion, Cahn-Hoffman $\boldsymbol{\xi}$-vector, shape derivative, thermodynamic variation.

AMS subject classifications. 74G65, 74G15, 74H15, 49Q10

1. Introduction.

Driven by capillarity effects, solid thin films sitting on a substrate are rarely stable and could exhibit complex morphological changes, e.g. the faceting [28, 29, 56], edge retraction [54, 14, 57, 58, 32], pinch-off [23, 31], fingering instabilities [30, 11, 18] and so on. This phenomenon, known as solid-state dewetting [51], has been widely observed across many thin film/substrate systems in materials science [28, 29, 32, 46]. Solid-state dewetting can be deleterious by fabricating the thin film structures, e.g., microelectronic and optoelectronic devices, thus destroying the reliability of the devices. On the other hand, it is advantageous and can be positively used to produce the well-controlled formation of an array of micro-/nanoscale particles, e.g., used in sensors [36, 2] and as catalysts for carbon [43] and semiconductor nanowire growth [45]. Recently, the solid-state dewetting has attracted considerable interest, and has been studied extensively from the experimental (e.g., [56, 57, 58, 1, 42, 20, 39, 38, 33]) and theoretical (e.g., [23, 48, 49, 52, 25, 24, 27, 6, 5, 14, 54, 32, 31, 30, 62]) points of view by many research groups. The understanding of its equilibrium patterns and kinetic morphology evolution characteristics could provide some important knowledge to develop new experimental methods to control solid-state dewetting [34], and enhance its potential applications in thin film technologies.

Modeling solid-state dewetting has been one of active research areas and become

*School of Mathematics and Statistics & Computational Science Hubei Key Laboratory, Wuhan University, Wuhan 430072, P.R. China (jiangwei1007@whu.edu.cn). This author's research was supported by the National Natural Science Foundation of China Nos. 11871384 and 91630313, and the Natural Science Foundation of Hubei Province Grant No. 2018CFB466.

†Corresponding author: Department of Mathematics, National University of Singapore, Singapore 119076 (quanzhao90@u.nus.edu). This author's research was supported by the Ministry of Education of Singapore grant R-146-000-247-114.

‡Department of Mathematics, National University of Singapore, Singapore 119076 (matbaowz@nus.edu.sg, URL: http://www.math.nus.edu.sg/~bao/). This author's research was supported by the Ministry of Education of Singapore grant R-146-000-247-114 and the National Natural Science Foundation of China No.91630207.

increasingly urgent in decades. Surface diffusion flow and contact line migration are recognised as the two main kinetic features for the evolution of solid-state dewetting. The first sharp-interface model dated back to 1986, when Srolovitz and Safran [49] proposed a model to study the hole growth in solid-state dewetting under the three assumptions, i.e., isotropic surface energy, small slope profile and cylindrical symmetry. The phase field approach has also been utilized to model solid-state dewetting, and the derived models can naturally capture the complex topology change during the evolution [23, 3]. Moreover, many other approaches have been proposed and discussed in order to include the anisotropic surface energy effects, such as the discrete model [14], a kinetic Monte Carlo model [41, 15], a crystalline model [10, 61] and continuum models based on partial differential equations (PDEs) [52, 25, 6, 17].

Under isothermal conditions, the equilibrium shape for a free-standing solid particle can be formulated by minimizing the interfacial energy subject to the constraint of a constant volume:

$$\min_{\Omega} W := W(S) = \int_S \gamma(\mathbf{n})\, dS \quad \text{s.t.} \quad |\Omega| = \text{const}, \tag{1.1}$$

where Ω is the enclosed domain by a closed surface S, and $\gamma(\mathbf{n})$ is the surface energy (density) with $\mathbf{n} = (n_1, n_2, n_3)^T$ representing the crystallographic orientation. Based on the γ-plot, the equilibrium shape can be geometrically constructed via the well-known Wulff (Gibbs-Wulff) construction [55]. The resulted Wulff shape, is the inner convex region bounded by all planes that are perpendicular to orientation $\mathbf{n}$ and at a distance of $\gamma(\mathbf{n})$ from the origin. The Winterbottom construction [53] was subsequently proposed to treat the substrate case by truncating the Wulff shape with a flat plane, and the distance of the plan depends on the wettability of the substrate (substrate energy). On the other hand, many theories [8, 9] demonstrate that the derivatives of $\gamma(\mathbf{n})$ play an important role in investigating the dynamics and equilibrium for anisotropic interface problems. In 1972, Cahn and Hoffman developed the theory of $\boldsymbol{\xi}$-vector [22, 8] to describe the surface energy density of the solid materials. It is defined based on a homogeneous extension of γ:

$$\boldsymbol{\xi}(\mathbf{n}) = \nabla\hat{\gamma}(\mathbf{p})\Big|_{\mathbf{p}=\mathbf{n}}, \text{ with } \hat{\gamma}(\mathbf{p}) = |\mathbf{p}|\gamma\left(\frac{\mathbf{p}}{|\mathbf{p}|}\right), \quad \forall \mathbf{p} \in \mathbb{R}^3\backslash\{\mathbf{0}\}, \tag{1.2}$$

where $|\mathbf{u}| := \sqrt{u_1^2 + u_2^2 + u_3^2}$ for $\mathbf{u} = (u_1, u_2, u_3)^T \in \mathbb{R}^3$. Under this extension, $\hat{\gamma}$ satisfies

$$\hat{\gamma}(\lambda\mathbf{p}) = |\lambda|\hat{\gamma}(\mathbf{p}), \qquad \nabla\hat{\gamma}(\mathbf{p}) \cdot \mathbf{p} = \hat{\gamma}(\mathbf{p}), \quad \forall \lambda \neq 0, \mathbf{p} \in \mathbb{R}^3\backslash\{\mathbf{0}\}. \tag{1.3}$$

Compared to the traditional use of scalar function γ (or γ-plot), $\boldsymbol{\xi}$-vector formulation has some advantages in the description of equilibrium shapes and thermodynamic evolution for crystalline interfaces. Because the magnitude of the normal component for $\boldsymbol{\xi}$ equals to $\gamma(\mathbf{n})$ (By (1.3), we have $\boldsymbol{\xi} \cdot \mathbf{n} = \gamma(\mathbf{n})$), $\boldsymbol{\xi}$-plot shares similar geometry with the Wulff shape [8, 40]. The $\boldsymbol{\xi}$-plot can be regarded as the mathematical representation of the equilibrium shape for weakly anisotropic case (when $1/\gamma$-plot is convex). Fig. 1.1 depicts the γ-plot,$1/\gamma$-plot and $\boldsymbol{\xi}$-plot for four different types of anisotropies: (a) the isotropic surface energy, i.e., $\gamma(\mathbf{n}) \equiv 1$; (b) cubic surface energy $\gamma(\mathbf{n}) = 1 + a[n_1^4 + n_2^4 + n_3^4]$ with a representing the degree of anisotropy; (c) ellipsoidal surface energy $\gamma(\mathbf{n}) = \sqrt{a_1^2 n_1^2 + a_2^2 n_2^2 + a_3^2 n_3^2}$; (d) "cusped" surface energy defined as

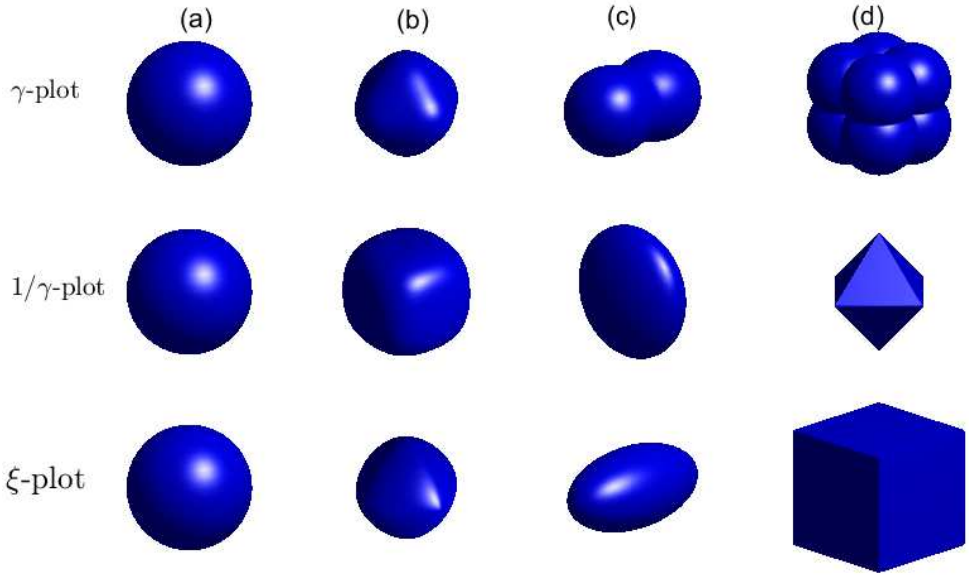

FIG. 1.1. *γ-plot, $1/\gamma$-plot and $\boldsymbol{\xi}$-plot for different anisotropies: (a) isotropic surface energy; (b) cubic anisotropic surface energy defined as $\gamma(\mathbf{n}) = 1 + 0.3(n_1^4 + n_2^4 + n_3^4)$; (c) ellipsoidal surface energy $\gamma(\mathbf{n}) = \sqrt{4n_1^2 + n_2^2 + n_3^2}$; (d) "cusped" surface energy defined as $\gamma(\mathbf{n}) = |n_1| + |n_2| + |n_3|$.*

$\gamma(\mathbf{n}) = |n_1| + |n_2| + |n_3|$. In the application of materials science, the surface energy is usually piecewise smooth and has some "cusped" points, where it is not differentiable [40, 19]. A typical example is the "cusped" surface energy defined above. For these cases, we can regularize the surface energy with a small parameter $0 < \varepsilon \ll 1$ to ensure the use of sharp-interface kinetic model in this paper, i.e.,

$$\gamma(\mathbf{n}) = \sqrt{\varepsilon^2 + (1-\varepsilon^2)n_1^2} + \sqrt{\varepsilon^2 + (1-\varepsilon^2)n_2^2} + \sqrt{\varepsilon^2 + (1-\varepsilon^2)n_3^2}. \tag{1.4}$$

The Cahn-Hoffman $\boldsymbol{\xi}$-vector has been recently utilized to describe the solid-state dewetting problem in two dimensions (2D) [26]. Based on the thermodynamic variation, the authors derived sharp-interface models via the Cahn-Hoffman $\boldsymbol{\xi}$-vector formulation for describing the evolution of solid-state dewetting. In this scenario, the moving interface is described as a parameterization over a time-independent domain, and the variation is performed by considering an infinitesimal perturbation with respect to an open curve. However, performing the thermodynamic variation for the 3D problem by using the approach of parameterized surfaces could be very different. Firstly, the calculations of the energy variation via surface parameterization are tedious and awkward. Secondly, for the solid-state dewetting problem, the infinitesimal perturbation to a surface in the tangential direction plays an important role in investigating the contact line migration along the substrate [25, 5]. These difficulties eliminate the possibility of treating the problem with the classic approach of parameterized surface or simply doing a normal perturbation. In the literature, the shape optimization problem is popular in the design and construction of industrial structures, and the speed method and shape derivatives have been widely utilized to perform the shape sensitivity analysis of such shape optimization problems [47, 21, 13]. This approach avoids the parameterization of a surface on a fixed reference domain

and is able to deal with perturbations along arbitrary directions.

Therefore, based on the $\boldsymbol{\xi}$-vector formulation and the speed method, the objectives of this paper are as follows: (i) to calculate the first variation of the energy functional for solid-state dewetting in 3D; (ii) to provide a rigorous derivation of the thermodynamic description of the equilibrium shape for solid-state dewetting in 3D; (iii) to develop a kinetic sharp-interface model which includes the surface diffusion and contact line migration for simulating morphology evolution in 3D; and (iv) to present numerical simulations to investigate important characteristics of the morphological evolution for solid-state dewetting observed in experiments.

The rest of the paper is organized as follows. In Section 2, we briefly introduce the speed method and sharp derivatives, and then apply them for calculating the first variation of the total free energy functional. In Section 3, we rigorously derive the necessary conditions for the equilibrium shape and explicitly give an expression for the equilibrium shape by using a parameterized formula. In Section 4, based on thermodynamic variation, a sharp-interface model is proposed for simulating solid-state dewetting of thin films in 3D. Subsequently, we perform some numerical simulations to demonstrate the accuracy and efficacy of our proposed model in Section 5. Finally, we draw some conclusions in Section 6.

2. Thermodynamic variation. The solid-state dewetting problem can be illustrated as Fig. 2.1, where a solid thin film (in blue) can dewet or agglomerate on a flat rigid substrate (in gray) due to capillarity effects. The total interfacial free energy of the system can be written as [5, 26]

$$W = \int_{S_{FV}} \gamma_{FV}\, dS_{FV} + \underbrace{\int_{S_{FS}} \gamma_{FS}\, dS_{FS} + \int_{S_{VS}} \gamma_{VS}\, dS_{VS}}_{\text{Substrate energy}}, \tag{2.1}$$

where $S_{FV} := S$, S_{FS} and S_{VS} represent the film/vapor, film/substrate and and

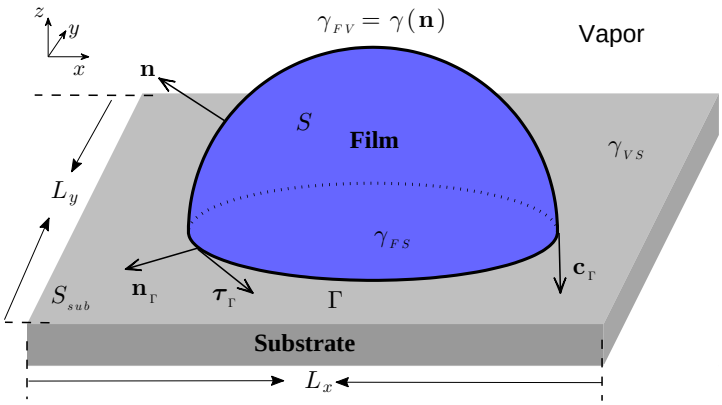

FIG. 2.1. *A schematic illustration of the solid-state dewetting of a solid thin film (in blue) on a flat, rigid substrate (in gray) in three dimensions.*

vapor/substrate interfaces, respectively, and γ_{FV}, γ_{FS} and γ_{VS} represent the corresponding surface energy densities. In solid-state dewetting problems, we often assume that γ_{FS}, γ_{VS} are two constants, and γ_{FS} is a function of the orientation of the

film/vapor interface, i.e., $\gamma_{FV} := \gamma(\mathbf{n})$ with $\mathbf{n}$ representing the unit normal vector of the film/vapor interface, which points outwards to the vapor phase. The film/vapor interface is here described by an open two-dimensional surface S with boundary Γ (i.e., the contact line), which is a closed plane curve in the flat substrate S_{sub}.

Assume that we consider a bounded domain with size $L_x \times L_y$ on the substrate (shown in Fig. 2.1), and we label the surface area enclosed by the contact line Γ as $A(\Gamma)$, then the total interfacial free energy of the system can be calculated as

$$\begin{aligned} W &= \int_{S_{FV}} \gamma_{FV}\, dS_{FV} + \int_{S_{FS}} \gamma_{FS}\, dS_{FS} + \int_{S_{VS}} \gamma_{VS}\, dS_{VS} \\ &= \int_S \gamma(\mathbf{n})\, dS + A(\Gamma)\gamma_{FS} + (L_x L_y - A(\Gamma))\, \gamma_{VS} \\ &= \int_S \gamma(\mathbf{n})\, dS + (\gamma_{FS} - \gamma_{VS})A(\Gamma) + L_x L_y \gamma_{VS}. \end{aligned} \tag{2.2}$$

By dropping off the constant term, we can simplify the total interfacial free energy as the following two parts, i.e., the film/vapor interface energy term W_{int} and the substrate energy term W_{sub},

$$W = W_{\text{int}} + W_{\text{sub}} = \int_S \gamma(\mathbf{n})\, dS + (\gamma_{FS} - \gamma_{VS})A(\Gamma). \tag{2.3}$$

As shown in Fig. 2.1, we introduce three unit vectors $\mathbf{n}_\Gamma$, $\boldsymbol{\tau}_\Gamma$ and $\mathbf{c}_\Gamma$, which are defined along the boundary Γ. More precisely, $\mathbf{n}_\Gamma$ is the outer unit normal vector of the plane curve Γ on the substrate S_{sub}; $\boldsymbol{\tau}_\Gamma$ is the unit tangent vector of Γ on the substrate surface S_{sub}, which points anticlockwise when looking from top to bottom; $\mathbf{c}_\Gamma$ is called as the co-normal vector, which is normal to Γ and tangent to the surface S, and points outwards to the vapor phase. For any point $\mathbf{x} \in S$ (with $\mathbf{x} = (x_1, x_2, x_3)^T$ or $(x, y, z)^T$), if we label $\mathcal{T}_{\mathbf{x}} S$ and $\mathcal{N}_{\mathbf{x}} S$ as the tangent and normal vector spaces to S at $\mathbf{x}$, respectively, then the following properties are valid,

$$\begin{aligned} &\boldsymbol{\tau}_\Gamma(\mathbf{x}) \in \mathcal{T}_{\mathbf{x}} S, \qquad \boldsymbol{\tau}_\Gamma(\mathbf{x}) /\!\!/ S_{\text{sub}}, \qquad \boldsymbol{\tau}_\Gamma(\mathbf{x}) \perp \mathbf{c}_\Gamma(\mathbf{x}), \quad \forall \mathbf{x} \in \Gamma, \\ &\mathbf{c}_\Gamma(\mathbf{x}) \in \mathcal{T}_{\mathbf{x}} S, \qquad \mathbf{n}_\Gamma(\mathbf{x}) /\!\!/ S_{\text{sub}}, \qquad \mathbf{n}_\Gamma(\mathbf{x}) \perp \boldsymbol{\tau}_\Gamma(\mathbf{x}), \quad \forall \mathbf{x} \in \Gamma. \end{aligned} \tag{2.4}$$

2.1. Differential operators on manifolds. We start by introducing some basic knowledge about surface calculus and differential geometry. For more details, please refer to [12, 16].

DEFINITION 2.1. *Suppose $S \subset \mathbb{R}^3$ is a two-dimensional smooth manifold, and a function f is defined on S such that $f \in C^2(S)$. Let $\mathbf{n} = (n_1,\ n_2,\ n_3)^T$ be the unit normal vector of S, and $\bar{f}$ be an extension of f in the neighbourhood of S such that $\bar{f}$ is differentiable, then the surface gradient of f on S is defined as*

$$\nabla_{\!S} f = \nabla \bar{f} - (\nabla \bar{f} \cdot \mathbf{n})\, \mathbf{n}, \tag{2.5}$$

with ∇ denoting the usual gradient in $\mathbb{R}^3$. It is easy to show that $\nabla_{\!S} f$ is independent of the extension of f and only dependent on the value of f on S. If we denote $\nabla_{\!S}$ as a vector operator

$$\nabla_{\!S} = (\underline{D}_1,\ \underline{D}_2,\ \underline{D}_3)^T, \tag{2.6}$$

then we can easily obtain

$$\underline{D}_i x_j = \delta_{ij} - n_i\, n_j, \qquad \forall 1 \le i,\, j \le 3, \tag{2.7}$$

where δ_{ij} is the Kronecker delta. The surface divergence of a vector-valued function $\mathbf{g} = (g_1,\ g_2,\ g_3)^T \in [C^1(S)]^3$ is defined as

$$\nabla_{_S} \cdot \mathbf{g} = \sum_{i=1}^{3} \underline{D}_i\, g_i. \tag{2.8}$$

Moreover, the Laplace-Beltrami operator on S can be expressed as

$$\Delta_{_S}\, f = \nabla_{_S} \cdot (\nabla_{_S}\, f) = \sum_{i=1}^{3} \underline{D}_i \underline{D}_i f. \tag{2.9}$$

In the definition of surface gradient, since the normal component has been subtracted from $\nabla \bar{f}$, $\nabla_{_S} f$ can be viewed as the tangential component of $\nabla \bar{f}$, and thus we have $\nabla_{_S} f(\mathbf{x}) \in \mathcal{T}_{\mathbf{x}}\, S,\ \forall \mathbf{x} \in S$.

On the other hand, the integration by parts on an open smooth surface S with smooth boundary Γ reads as (see Theorem 2.10 in [16], and we omit the proof here)

$$\int_S \nabla_{_S} f\ dS = \int_S f\, \mathcal{H}\, \mathbf{n}\ dS + \int_\Gamma f\, \mathbf{c}_{_\Gamma}\ d\Gamma, \tag{2.10}$$

where $\mathbf{n}$ and $\mathbf{c}_{_\Gamma}$ are the normal and co-normal vectors (shown in Fig. 2.1), respectively, and $\mathcal{H}$ is the mean curvature, which is defined as the surface divergence of the unit normal vector, i.e., $\mathcal{H} = \nabla_{_S} \cdot \mathbf{n}$. Furthermore, by using the product rule that $\nabla_{_S}(fg) = g\, \nabla_{_S} f + f\, \nabla_{_S} g$, we can obtain

$$\int_S g\, \nabla_{_S} f\ dS = -\int_S f\, \nabla_{_S} g\ dS + \int_S f\, g\, \mathcal{H}\, \mathbf{n}\ dS + \int_\Gamma f\, g\, \mathbf{c}_{_\Gamma}\ d\Gamma. \tag{2.11}$$

In a simple case, if S is a flat surface (i.e., $\mathcal{H} = 0$) with a plane boundary curve Γ, then Eq. (2.10) can be reduced to

$$\int_S \nabla_{_S} f\ dS = \int_\Gamma f\, \mathbf{c}_{_\Gamma}\ d\Gamma, \tag{2.12}$$

which is the Gauss-Green theorem in the multivariable calculus, because $\nabla_{_S} f$ collapses to the gradient of f in 2D, and $\mathbf{c}_{_\Gamma}$ collapses to the unit outer normal vector of Γ.

2.2. The speed method and shape derivative. In this section, the objective is to calculate the first variation of the energy (or shape) functional defined in (2.3). To this end, we first introduce an independent parameter $\epsilon \in [0, \epsilon_0)$ to parameterize a family of perturbations $\{D_\epsilon\}$ of a given domain $D \subset \mathbb{R}^3$, where the parameter ϵ controls the amplitude of the perturbation and ϵ_0 is the maximum perturbation amplitude. Furthermore, we assume that the domains $D \equiv D_0$ and D_ϵ for $\epsilon \in [0, \epsilon_0)$ have the same topological properties and regularity, e.g., D and D_ϵ for $\epsilon \in [0, \epsilon_0)$ are of class C^k with $k \geq 1$.

More precisely, we consider a bounded domain $D \subset \mathbb{R}^3$ with a piecewise smooth boundary ∂D, then we can construct a family of transformations T_ϵ, which are one-to-one, and T_ϵ maps D onto D_ϵ, i.e.,

$$T_\epsilon :\ D\ \rightarrow\ D_\epsilon, \qquad \epsilon \in [0, \epsilon_0), \tag{2.13}$$

where ϵ is the small perturbation parameter. Generally, we assume that: (i) T_ϵ and T_ϵ^{-1} belong to $C^k(\mathbb{R}^3, \mathbb{R}^3)$ for all $\epsilon \in [0, \epsilon_0)$ with $k \in \mathbb{N} \cup \{\infty\}$; and (ii) the mappings $\epsilon \rightarrow T_\epsilon(\mathbf{x})$ and $\epsilon \rightarrow T_\epsilon^{-1}(\mathbf{x})$ belongs to $C^1[0, \epsilon_0)$ for all $\mathbf{x} \in \mathbb{R}^3$ (with $\mathbf{x} = (x_1, x_2, x_3)^T$).

Given any point $\mathbf{X} \in \bar{D}$ (with $\mathbf{X} = (X_1, X_2, X_3)^T$) and $\epsilon \in [0, \epsilon_0)$, we can define the point $\mathbf{x} = T_\epsilon(\mathbf{X})$ which moves along the trajectory. Here, the point $\mathbf{X}$ represents the Lagrangian (or material) coordinate, while $\mathbf{x}$ is the Eulerian (or actual) coordinate. Therefore, the speed vector field $\mathbf{V}(\mathbf{x}, \epsilon)$ at point $\mathbf{x}$ is defined as

$$\mathbf{V}(\mathbf{x}, \epsilon) = \frac{\partial \mathbf{x}}{\partial \epsilon}(T_\epsilon^{-1}(\mathbf{x}), \epsilon). \tag{2.14}$$

On the other hand, the transformation T_ϵ can be uniquely determined by the speed vector field $\mathbf{V}$ via the following ordinary differential equation (ODE)

$$\begin{cases} \frac{d}{d\epsilon}\mathbf{x}(\mathbf{X}, \epsilon) = \mathbf{V}(\mathbf{x}(\mathbf{X}, \epsilon), \epsilon), \\ \mathbf{x}(\mathbf{X}, 0) = \mathbf{X}. \end{cases} \tag{2.15}$$

Therefore, the transformation T_ϵ and the smooth vector field $\mathbf{V}$ are uniquely determined by each other. For a smooth vector field $\mathbf{V}$, e.g., $\mathbf{V} \in C(C^k(\bar{D}, \mathbb{R}^3); [0, \epsilon_0))$, the equivalence between the transformation T_ϵ and the speed vector field $\mathbf{V}$ has been strictly established by Theorem 2.16 in [47]. In the following, we use $T_\epsilon(\mathbf{V})$ to denote the transformation associated with vector field $\mathbf{V}$. For simplicity, we also denote $\mathbf{V}_0 = \mathbf{V}(\mathbf{X}, 0)$.

Let $J(G)$ be a (shape) functional defined on a shape $G \subset \mathbb{R}^3$, where G could be a two-dimensional surface (e.g., S) or a three-dimensional domain (e.g., Ω). The first variation of the functional $J(G)$ at G in the direction of a speed vector field $\mathbf{V} \in C(C^k(\bar{D}, \mathbb{R}^3); [0, \epsilon_0))$ is given as the Eulerian derivative:

$$\delta J(G; \mathbf{V}) = \lim_{\epsilon \to 0} \frac{J(G_\epsilon) - J(G)}{\epsilon}, \tag{2.16}$$

where $G_\epsilon = T_\epsilon(\mathbf{V})(G)$. Based on the transformation, we can define the material derivative of a function over a shape.

Definition 2.2. *(Material derivatives, and refer to Def. 2.71 in [47]) The material derivative $\dot{\varphi}(G; \mathbf{V})$ of φ on the shape G in the direction of a speed vector field $\mathbf{V}$ is defined as*

$$\dot{\varphi}(G; \mathbf{V}) = \lim_{\epsilon \to 0} \frac{\varphi(G_\epsilon) \circ T_\epsilon(\mathbf{V}) - \varphi(G)}{\epsilon}, \tag{2.17}$$

where for $\mathbf{X} \in G$, $\varphi(G_\epsilon) \circ T_\epsilon(\mathbf{V}) = \varphi(T_\epsilon(\mathbf{X}))$.

Let $\Omega \subset \mathbb{R}^3$ be a bounded domain, and $J(\Omega) = \int_\Omega \psi(\Omega)\, d\Omega$ with $\psi \in W^{1,1}(\Omega)$. Using the change of variables $\mathbf{x} = T_\epsilon(\mathbf{V})(\mathbf{X})$ for $J(\Omega_\epsilon)$, we have

$$J(\Omega_\epsilon) = \int_\Omega \psi(\Omega_\epsilon) \circ T_\epsilon(\mathbf{V}) \zeta(\mathbf{X}, \epsilon)\, d\Omega, \tag{2.18}$$

where $\zeta(\mathbf{X}, \epsilon) = \det(\mathrm{DT}_\epsilon)$ with $\mathrm{DT}_\epsilon = \left(\frac{\partial \mathrm{T}_{\epsilon,\mathrm{i}}(\mathbf{V})}{\partial \mathrm{X}_\mathrm{j}}(\mathbf{X})\right)_{\mathrm{i,j}=1,2,3}$. By noting the fact that

$\zeta(\mathbf{X},0)=1$, $\frac{\partial\zeta(\mathbf{X},\epsilon)}{\partial\epsilon}\Big|_{\epsilon=0}=\nabla\cdot\mathbf{V}_0$ (see Proposition 2.44 in [47]), we have

$$\begin{aligned}\delta J(\Omega;\mathbf{V}) &= \lim_{\epsilon\to 0}\frac{J(\Omega_\epsilon)-J(\Omega)}{\epsilon}\\ &= \int_\Omega \lim_{\epsilon\to 0}\Big[\frac{\psi(\Omega_\epsilon)\circ T_\epsilon(\mathbf{V})\zeta(\mathbf{X},\epsilon)-\psi(\Omega)\circ T_0(\mathbf{V})\zeta(\mathbf{X},0)}{\epsilon}\Big]\,d\Omega\\ &= \int_\Omega\Big[\dot{\psi}(\Omega;\mathbf{V})\zeta(\mathbf{X},0)+\psi(\Omega)\frac{\partial\zeta(\mathbf{X},\epsilon)}{\partial\epsilon}\Big|_{\epsilon=0}\Big]\,d\Omega\\ &= \int_\Omega\dot{\psi}(\Omega;\mathbf{V})\,d\Omega+\int_\Omega\psi(\Omega)\nabla\cdot\mathbf{V}_0\,d\Omega. \qquad (2.19)\end{aligned}$$

We can define the shape derivative $\psi'(\Omega;\mathbf{V})$ of $\psi(\Omega)$ on Ω in the direction $\mathbf{V}$ as

$$\psi'(\Omega;\mathbf{V})=\dot{\psi}(\Omega;\mathbf{V})-\nabla\psi(\Omega)\cdot\mathbf{V}_0. \qquad (2.20)$$

Integration by parts for the second term of Eq. (2.19), we then obtain that

$$\delta J(\Omega;\mathbf{V})=\int_\Omega\psi'(\Omega;\mathbf{V})\,d\Omega+\int_{\partial\Omega}\psi(\Omega)\,\mathbf{V}_0\cdot\mathbf{n}\,d\Omega. \qquad (2.21)$$

If $\mathbf{V}_0\cdot\mathbf{n}=0$ on the boundary $\partial\Omega$, we obtain that the first variation of the functional reduces to

$$\delta J(\Omega;\mathbf{V})=\int_\Omega\psi'(\Omega;\mathbf{V})\,d\Omega. \qquad (2.22)$$

The material derivative can be regarded as the derivative with respect to the geometry in the moving coordinate systems. On the other hand, the shape derivative of ψ represents the derivative with respect to the geometry in the stationary coordinates by subtracting the term $\nabla\psi\cdot\mathbf{V}_0$. If $\psi\in W^{1,1}(\mathbb{R}^3)$ is independent on the geometric object Ω, then we have $\psi'(\Omega;\mathbf{V})=0$. Furthermore, for a function $\varphi(S)$ defined over a two-dimensional manifold S, we can define the shape derivative as follows.

Definition 2.3. *(Shape derivatives, and see Def. 2.88 in [47]) The shape derivative $\varphi'(S;\mathbf{V})$ of φ defined on S in the direction of a vector field $\mathbf{V}$ is defined as*

$$\varphi'(S;\mathbf{V})=\dot{\varphi}(S;\mathbf{V})-\nabla_{_S}\varphi(S)\cdot\mathbf{V}_0. \qquad (2.23)$$

This definition ensures that the shape derivative shows no dependence on the extension of φ in the near neighbourhood. We proposed the following proposition to show that the first variation of a functional on S is closely related to the shape derivative.

Proposition 2.1. *Let S be a two-dimensional manifold in $\bar{D}$ with smooth boundary Γ, and $\mathbf{V}$ be a speed vector field such that $\mathbf{V}\in C(C^k(\bar{D},\mathbb{R}^3);[0,\epsilon_0))$. $\varphi(S)\in W^{1,1}(S)$ is a function such that the material derivative $\dot{\varphi}(S;\mathbf{V})$ exists or exists in the weak sense and $\dot{\varphi}(S;\mathbf{V})\in L^1(S)$. Given the shape functional $J(S)=\int_S\varphi(S)\,dS$, we then have*

$$\delta J(S;\mathbf{V})=\int_S\dot{\varphi}(S;\mathbf{V})\,dS+\int_S\varphi(S)\nabla_{_S}\cdot\mathbf{V}_0\,dS. \qquad (2.24)$$

Furthermore, if the shape derivative $\varphi'(S;\mathbf{V})$ exists and $(\nabla_{_S}\varphi\cdot\mathbf{V}_0)\in L^1(S)$, we have

$$\delta J(S;\mathbf{V})=\int_S\varphi'(S;\mathbf{V})\,dS+\int_S\varphi(S)\mathcal{H}\mathbf{V}_0\cdot\mathbf{n}\,dS+\int_\Gamma\varphi(S)\mathbf{V}_0\cdot\mathbf{c}_{_\Gamma}\,d\Gamma. \qquad (2.25)$$

Proof. According to the change of variables $\mathbf{x} = T_\epsilon(\mathbf{V})(\mathbf{X})$, and by using the transformation $T_\epsilon(\mathbf{V})$, the shape functional $J(S_\epsilon)$ over the perturbed surfaces S can be expressed as follows:

$$J(S_\epsilon) = \int_{S_\epsilon} \varphi(S_\epsilon)\, dS_\epsilon = \int_S (\varphi \circ T_\epsilon(V))(\mathbf{X})\, \omega(\mathbf{X}, \epsilon)\, dS, \tag{2.26}$$

where $\omega(\mathbf{X}, \epsilon)$ is defined as

$$\omega(\mathbf{X}, \epsilon) = \det(\mathrm{DT}_\epsilon)\, |((\mathrm{DT}_\epsilon)^{-1})^{\mathrm{T}}\mathbf{n}|, \quad \text{with } \mathrm{DT}_\epsilon = \Big(\frac{\partial \mathrm{T}_{\epsilon,\mathrm{i}}(\mathbf{V})}{\partial \mathrm{X}_\mathrm{j}}(\mathbf{X})\Big)_{\mathrm{i,j}=1,2,3}. \tag{2.27}$$

Note that the following expressions hold according to the Lemma 2.49 in Page 80 of [47],

$$\omega(\mathbf{X}, 0) = 1, \qquad \frac{\partial \omega(\mathbf{X}, \epsilon)}{\partial \epsilon}\Big|_{\epsilon=0} = \nabla_{_S} \cdot \mathbf{V}_0. \tag{2.28}$$

Therefore, based on the definition of the first variation, we have

$$\begin{aligned}
\delta J(S; \mathbf{V}) &= \lim_{\epsilon \to 0} \frac{J(S_\epsilon) - J(S)}{\epsilon} \\
&= \int_S \lim_{\epsilon \to 0} \Big[\frac{\varphi(S_\epsilon) \circ T_\epsilon(V)\omega(\mathbf{X}, \epsilon) - \varphi \circ T_0(V)\omega(\mathbf{X}, 0)}{\epsilon} \Big]\, dS \\
&= \int_S \dot{\varphi}(S; \mathbf{V})\omega(\mathbf{X}, 0)\, dS + \int_S \varphi(S) \frac{\partial \omega(\mathbf{X}, \epsilon)}{\partial \epsilon}\Big|_{\epsilon=0}\, dS \\
&= \int_S \dot{\varphi}(S; \mathbf{V})\, dS + \int_S \varphi(S) \nabla_{_S} \cdot \mathbf{V}_0\, dS. \qquad (2.29)
\end{aligned}$$

Furthermore, by using the integration by parts and also making use of Eq. (2.23), we also obtain

$$\begin{aligned}
\delta J(S; \mathbf{V}) &= \int_S \dot{\varphi}(S; \mathbf{V}_0)\, dS - \int_S \nabla_{_S} \varphi(S) \cdot \mathbf{V}_0\, dS + \int_S \varphi(S) \mathcal{H} \mathbf{V}_0 \cdot \mathbf{n}\, dS \\
&\quad + \int_\Gamma \varphi(S) \mathbf{V}_0 \cdot \mathbf{c}_{_\Gamma}\, d\Gamma \\
&= \int_S \varphi'(S; \mathbf{V})\, dS + \int_S \varphi(S) \mathcal{H} \mathbf{V}_0 \cdot \mathbf{n}\, dS + \int_\Gamma \varphi(S) \mathbf{V}_0 \cdot \mathbf{c}_{_\Gamma}\, d\Gamma,
\end{aligned}$$

which completes the proof. □

From Proposition 2.1, we have shown that the shape derivative $\varphi'(S; \mathbf{V})$ is an important tool to derive the first variation of a shape functional over a surface. We can assume that ψ is a function defined on the domain Ω, such that its restriction on S is equal to function $\varphi(S)$, namely

$$\psi(\Omega)\Big|_S = \varphi(S). \tag{2.30}$$

By using Eq. (2.20) and Eq. (2.24), we can reformulate Eq. (2.25) in terms of the extension function ψ as

$$\delta J(S; \mathbf{V}) = \int_S \psi'(\Omega; \mathbf{V})\Big|_S\, dS + \int_S \big(\partial_{\mathbf{n}} \psi + \psi \mathcal{H}\big) \mathbf{V}_0 \cdot \mathbf{n}\, dS + \int_\Gamma \psi \mathbf{V}_0 \cdot \mathbf{c}_{_\Gamma}\, d\Gamma. \tag{2.31}$$

In the following, we will apply Eq. (2.31) for calculating the first variation of the energy (or shape) functional defined in (2.3), where the integrand is the surface energy density $\gamma(\mathbf{n})$. To calculate the shape derivatives and obtain the first variation, we shall make use of the signed distance function, which is a powerful tool in shape sensitivity analysis. Consider a closed domain $\Omega \subset \mathbb{R}^3$ with a smooth boundary surface $\partial\Omega$, and then the signed distance function is defined as

$$b(\mathbf{x}) = \begin{cases} \mathrm{d}(\mathbf{x}, \partial\Omega), & \forall \mathbf{x} \in \mathbb{R}^3 \backslash \Omega, \\ 0, & \forall \mathbf{x} \in \partial\Omega, \\ -\mathrm{d}(\mathbf{x}, \partial\Omega), & \forall \mathbf{x} \in \Omega. \end{cases} \tag{2.32}$$

Here, $\mathrm{d}(\mathbf{x}, \partial\Omega) = \inf_{\mathbf{y}\in\partial\Omega} ||\mathbf{x} - \mathbf{y}||$. The signed distance function $b(\mathbf{x})$ can be used to determine the unit outer normal vector $\mathbf{n}$ and the mean curvature $\mathcal{H}$ on the boundary surface $\partial\Omega$. More precisely, we can extend the functions $\mathbf{n}$ and $\mathcal{H}$ which are defined on $\partial\Omega$ in terms of $b(\mathbf{x})$ in a tubular neighbourhood such that

$$\mathbf{n}(\mathbf{x}) = \nabla b(\mathbf{x})\Big|_{\partial\Omega}, \qquad \mathcal{H}(\mathbf{x}) = \Delta b(\mathbf{x})\Big|_{\partial\Omega}, \qquad \forall \mathbf{x} \in \partial\Omega. \tag{2.33}$$

The shape derivative of the signed distance function in the direction of a vector field $\mathbf{V}$ is calculated as $b'(\Omega; \mathbf{V}) = -\mathbf{V}_0 \cdot \mathbf{n}$ (see Section 3 in [21] for details). Moreover, based on the extension, the shape derivatives of the two extension functions restricted on $\partial\Omega$ are also obtained in [21], i.e.,

$$\mathbf{n}'(\Omega; \mathbf{V})\Big|_{\partial\Omega} = -\nabla_{\!S}(\mathbf{V}_0 \cdot \mathbf{n}), \qquad \mathcal{H}'(\Omega; \mathbf{V})\Big|_{\partial\Omega} = -\Delta_S(\mathbf{V}_0 \cdot \mathbf{n}). \tag{2.34}$$

2.3. First variation. By applying Eq. (2.31) and making use of the shape derivative of the unit outer normal vector, we obtain the following lemma.

LEMMA 2.1. *Assume that $S \subset \bar{D}$ is a two dimensional manifold of class C^2 with smooth boundary Γ. Let $\mathbf{n}$ be the unit outer normal vector of S, and $\mathbf{V}$ be a speed vector field such that $\mathbf{V} \in C(C^k(\bar{D}, \bar{D}); [0, \epsilon_0))$. If the shape functional $J(S) = \int_S \gamma(\mathbf{n})\, dS$ with a surface energy (density) $\gamma(\mathbf{n})$, then the first variation of $J(S)$ is given as*

$$\delta J(S; \mathbf{V}) = \int_S (\nabla_{\!S} \cdot \boldsymbol{\xi})\, (\mathbf{V}_0 \cdot \mathbf{n})\, dS + \int_\Gamma \mathbf{V}_0 \cdot \mathbf{c}_{\Gamma}^{\gamma}\, d\Gamma, \tag{2.35}$$

where $\boldsymbol{\xi} := \boldsymbol{\xi}(\mathbf{n})$ is the Cahn-Hoffman vector, which is defined previously in Eq. (1.2)*, and $\mathbf{V}_0 \cdot \mathbf{n}$ represents the deformation velocity along the outer normal direction of the interface S, and the vector $\mathbf{c}_{\Gamma}^{\gamma} := (\boldsymbol{\xi} \cdot \mathbf{n})\, \mathbf{c}_{\Gamma} - (\boldsymbol{\xi} \cdot \mathbf{c}_{\Gamma})\, \mathbf{n}$ with $\mathbf{c}_{\Gamma}$ representing the unit co-normal vector (shown in Fig. 2.1).*

Proof. We firstly assume $\hat{\gamma}$ is a homogeneous extension of γ,

$$\hat{\gamma}(\mathbf{p}) = |\mathbf{p}| \gamma\left(\frac{\mathbf{p}}{|\mathbf{p}|}\right), \quad \forall\, \mathbf{p} \in \mathbb{R}^3 \backslash \{\mathbf{0}\}, \tag{2.36}$$

where the definition domain of the function $\gamma(\mathbf{n})$ changes from unit vectors $\mathbf{n}$ to arbitrary non-zero vectors $\mathbf{p} \in \mathbb{R}^3$.

We next consider a bounded domain $\Omega \subset \mathbb{R}^3$ such that $S \subset \partial\Omega$. Then, based on the signed distance function defined in (2.32), we can define $\nabla b(x) \in \mathbb{R}^3$ as an extension of the normal vector $\mathbf{n}$ in the neighbourhood of S. Thus we can reformulate

$$J(S) = \int_S \hat{\gamma}\big(\nabla b(\mathbf{x})\big)\Big|_S\, dS = \int_S \psi(\Omega)\Big|_S\, dS, \tag{2.37}$$

with $\psi(\Omega) := \hat{\gamma}\big(\nabla b(\mathbf{x})\big)$. Using the chain rule for shape derivatives and the definition of Cahn-Hoffman $\boldsymbol{\xi}$-vector in Eq. (1.2), we conclude that the following expression holds,

$$\psi'(\Omega;\mathbf{V})\Big|_S = \nabla\hat{\gamma}\big(\nabla b(\mathbf{x})\big)\Big|_S \cdot \mathbf{n}'(\Omega;\mathbf{V})\Big|_S = -\boldsymbol{\xi}\cdot\nabla_S(\mathbf{V}_0\cdot\mathbf{n}). \tag{2.38}$$

Moreover, By noting the fact $|\nabla b(\mathbf{x})| = 1$, we obtain

$$\partial_{\mathbf{n}}\psi\Big|_S = \boldsymbol{\xi}\cdot\big((\nabla\nabla b(\mathbf{x}))\ \nabla b(\mathbf{x})\big)\Big|_S = 0, \tag{2.39}$$

where $\nabla\nabla b(\mathbf{x}) \in \mathbb{R}^{3\times 3}$. By making use of Eq. (2.31) and combining Eq. (2.38) and (2.39), we immediately have

$$\begin{aligned}\delta J(S;\mathbf{V}) \ &= -\int_S \boldsymbol{\xi}\cdot\nabla_S(\mathbf{V}_0\cdot\mathbf{n})\,dS + \int_S \gamma(\mathbf{n})\,(\mathbf{V}_0\cdot\mathbf{n})\,\mathcal{H}\,dS + \int_\Gamma \gamma(\mathbf{n})\,(\mathbf{V}_0\cdot\mathbf{c}_\Gamma)\,d\Gamma \\ &:= I + II + III. \end{aligned} \tag{2.40}$$

For the first term, by using integration by parts, we obtain

$$I = \int_S (\nabla_S\cdot\boldsymbol{\xi})\,(\mathbf{V}_0\cdot\mathbf{n})\,dS - \int_S (\boldsymbol{\xi}\cdot\mathbf{n})\,(\mathbf{V}_0\cdot\mathbf{n})\,\mathcal{H}\,dS - \int_\Gamma (\boldsymbol{\xi}\cdot\mathbf{c}_\Gamma)\,(\mathbf{V}_0\cdot\mathbf{n})\,d\Gamma. \tag{2.41}$$

Based on Eq. (1.3), we have $\gamma(\mathbf{n}) = \boldsymbol{\xi}\cdot\mathbf{n}$. Thus we can rewrite

$$II = \int_S (\boldsymbol{\xi}\cdot\mathbf{n})\,(\mathbf{V}_0\cdot\mathbf{n})\mathcal{H}\,dS. \tag{2.42}$$

$$III = \int_\Gamma (\boldsymbol{\xi}\cdot\mathbf{n})\,(\mathbf{V}_0\cdot\mathbf{c}_\Gamma)\,d\Gamma. \tag{2.43}$$

Finally, by combining the above three terms together, we immediately have

$$\begin{aligned}\delta J(S;\mathbf{V}) &= \int_S (\nabla_S\cdot\boldsymbol{\xi})\,(\mathbf{V}_0\cdot\mathbf{n})\,dS + \int_\Gamma \Big[(\boldsymbol{\xi}\cdot\mathbf{n})\,\mathbf{c}_\Gamma - (\boldsymbol{\xi}\cdot\mathbf{c}_\Gamma)\,\mathbf{n}\Big]\cdot\mathbf{V}_0\,d\Gamma \\ &= \int_S (\nabla_S\cdot\boldsymbol{\xi})\ (\mathbf{V}_0\cdot\mathbf{n})\,dS + \int_\Gamma \mathbf{c}_\Gamma^\gamma\cdot\mathbf{V}_0\,d\Gamma, \end{aligned} \tag{2.44}$$

with $\mathbf{c}_\Gamma^\gamma = (\boldsymbol{\xi}\cdot\mathbf{n})\,\mathbf{c}_\Gamma - (\boldsymbol{\xi}\cdot\mathbf{c}_\Gamma)\,\mathbf{n}$. □

By using the above Lemma, we can easily obtain the first variation of the energy functional for solid-state dewetting problems defined in (2.3).

THEOREM 2.1. *The first variation of the free energy (or shape) functional* (2.3) *used in solid-state dewetting problems with respect to a smooth vector field* $\mathbf{V}$ *can be written as:*

$$\delta W(S;\mathbf{V}) = \int_S (\nabla_S\cdot\boldsymbol{\xi})\ (\mathbf{V}_0\cdot\mathbf{n})\,dS + \int_\Gamma (\mathbf{c}_\Gamma^\gamma\cdot\mathbf{n}_\Gamma + \gamma_{FS} - \gamma_{VS})(\mathbf{V}_0\cdot\mathbf{n}_\Gamma)\,d\Gamma. \tag{2.45}$$

Proof. From (2.3), we observe that the total free energy consists of two parts: the film/vapor interface energy W_{int} and the substrate energy part W_{sub}. First, by using Lemma. 2.1, we can directly obtain the first variation of the film/vapor interface energy W_{int} as follows,

$$\delta W_{\text{int}}(S;\mathbf{V}) = \int_S (\nabla_S\cdot\boldsymbol{\xi})\,(\mathbf{V}_0\cdot\mathbf{n})\,dS + \int_\Gamma \mathbf{V}_0\cdot\mathbf{c}_\Gamma^\gamma\,d\Gamma. \tag{2.46}$$

Here, $\mathbf{c}_\Gamma^\gamma$ is a linear combination of $\mathbf{c}_\Gamma$ and $\mathbf{n}$, which is defined on the contact line Γ. Therefore, as shown in Fig. 2.1, we have

$$\mathbf{c}_\Gamma \perp \boldsymbol{\tau}_\Gamma, \quad \mathbf{n} \perp \boldsymbol{\tau}_\Gamma \quad \Rightarrow \quad \mathbf{c}_\Gamma^\gamma \perp \boldsymbol{\tau}_\Gamma. \tag{2.47}$$

For solid-state dewetting problems studied in this paper, we assume that the contact line Γ must move along the substrate plane $S_{\rm sub}$, i.e.,

$$T_\epsilon\Gamma \subset S_{\rm sub}, \qquad \mathbf{V}_0(\mathbf{x}) /\!\!/ S_{\rm sub}, \qquad \forall \mathbf{x} \in \Gamma. \tag{2.48}$$

Therefore, for any $\mathbf{x} \in \Gamma$, $\mathbf{V}_0(\mathbf{x})$ can be decomposed into two vectors along the directions $\mathbf{n}_\Gamma$ and $\boldsymbol{\tau}_\Gamma$, i.e., $\mathbf{V}_0(\mathbf{x}) = k_1\mathbf{n}_\Gamma + k_2\boldsymbol{\tau}_\Gamma$, where k_1 and k_2 represent the corresponding components. By making use of (2.47), we can obtain

$$\begin{aligned}\mathbf{V}_0(\mathbf{x}) \cdot \mathbf{c}_\Gamma^\gamma &= (k_1\mathbf{n}_\Gamma + k_2\boldsymbol{\tau}_\Gamma) \cdot \mathbf{c}_\Gamma^\gamma = k_1(\mathbf{n}_\Gamma \cdot \mathbf{c}_\Gamma^\gamma) \\ &= (\mathbf{V}_0(\mathbf{x}) \cdot \mathbf{n}_\Gamma)\,(c_\Gamma^\gamma \cdot \mathbf{n}_\Gamma), \qquad \forall \mathbf{x} \in \Gamma.\end{aligned}$$

Thus we can reformulate (2.46) as

$$\delta W_{\rm int}(S;\mathbf{V}) = \int_S (\nabla_{_S} \cdot \boldsymbol{\xi})\,(\mathbf{V}_0 \cdot \mathbf{n})\,dS + \int_\Gamma (\mathbf{c}_\Gamma^\gamma \cdot \mathbf{n}_\Gamma)(\mathbf{V}_0 \cdot \mathbf{n}_\Gamma)\,d\Gamma. \tag{2.49}$$

On the other hand, we can rewrite the substrate energy $W_{\rm sub}$ as

$$W_{\rm sub} = (\gamma_{_{FS}} - \gamma_{_{VS}})A(\Gamma) = (\gamma_{_{FS}} - \gamma_{_{VS}}) \int_{S_{_{FS}}} dS_{_{FS}}. \tag{2.50}$$

By using Lemma 2.1, and noting that the integrand is a constant and $S_{_{FS}}$ is a flat surface with a plane boundary curve Γ (i.e., $\mathcal{H} = 0$ and $\mathbf{n}_\Gamma$ is the unit co-normal vector of the flat surface $S_{_{FS}}$), we directly have

$$\delta W_{\rm sub}(S;\mathbf{V}) = (\gamma_{_{FS}} - \gamma_{_{VS}}) \int_\Gamma \mathbf{V}_0 \cdot \mathbf{n}_\Gamma\, d\Gamma. \tag{2.51}$$

By combining Eqs. (2.49) and (2.51), we obtain the following conclusion

$$\delta W(S;\mathbf{V}) = \int_S (\nabla_{_S} \cdot \boldsymbol{\xi})\,(\mathbf{V}_0 \cdot \mathbf{n})\,dS + \int_\Gamma (\mathbf{c}_\Gamma^\gamma \cdot \mathbf{n}_\Gamma + \gamma_{_{FS}} - \gamma_{_{VS}})(\mathbf{V}_0 \cdot \mathbf{n}_\Gamma)\,d\Gamma, \tag{2.52}$$

which completes the proof. □

3. Equilibrium shapes. The equilibrium shape of the solid-state dewetting problem can be stated as follows [5]:

$$\min_\Omega W := W(S) = \int_S \gamma(\mathbf{n})\,dS + (\gamma_{_{FS}} - \gamma_{_{VS}})A(\Gamma) \quad \text{s.t.} \quad |\Omega| = \mathrm{C}, \tag{3.1}$$

where $C > 0$ is a prescribed constant representing the total volume of the dewetted particle, and Ω represents the domain (or the particle) enclosed by the interface S and the substrate plane $S_{\rm sub}$.

The Lagrangian for the above optimization problem can be defined as

$$L(S,\lambda) = \int_S \gamma(\mathbf{n})\,dS + (\gamma_{_{FS}} - \gamma_{_{VS}})A(\Gamma) - \lambda(|\Omega| - C), \tag{3.2}$$

with λ representing the Lagrange multiplier. The first variation of the total volume term can be obtained by simply choosing the integrand $\psi(\mathbf{x}) \equiv 1, \forall\, \mathbf{x} \in \Omega$ in Eq. (2.21). Therefore, by combining with Eq. (2.45), the first variation of the Lagrangian with respect to a smooth vector field $\mathbf{V}$ can be given as

$$\delta L(S, \lambda; \mathbf{V}) = \int_S (\nabla_s \cdot \boldsymbol{\xi} - \lambda)(\mathbf{V}_0 \cdot \mathbf{n})\, dS + \int_\Gamma (\mathbf{c}_\Gamma^\gamma \cdot \mathbf{n}_\Gamma + \gamma_{FS} - \gamma_{VS})(\mathbf{V}_0 \cdot \mathbf{n}_\Gamma)\, d\Gamma. \tag{3.3}$$

Based on the above first variation, we have the following lemma which yields the necessary conditions for the equilibrium shape of solid-state dewetting problem.

LEMMA 3.1. *Assume that a two-dimensional manifold S_e with smooth boundary Γ_e is the equilibrium shape of the solid-state dewetting problem* (3.1)*, then the following conditions must be satisfied*

$$\nabla_{S_e} \cdot \boldsymbol{\xi} = \lambda, \ \text{on } S_e. \tag{3.4a}$$

$$\mathbf{c}_\Gamma^\gamma \cdot \mathbf{n}_\Gamma + \gamma_{FS} - \gamma_{VS} = 0, \ \text{on } \Gamma_e. \tag{3.4b}$$

where the constant λ is determined by the prescribed total volume, i.e., the constant C.

Proof. If S_e is the equilibrium shape, then Eq. (3.3) *must vanish at $S = S_e$ for any smooth vector field $\mathbf{V}$. Thus we immediately obtain the above two conditions.* ∎

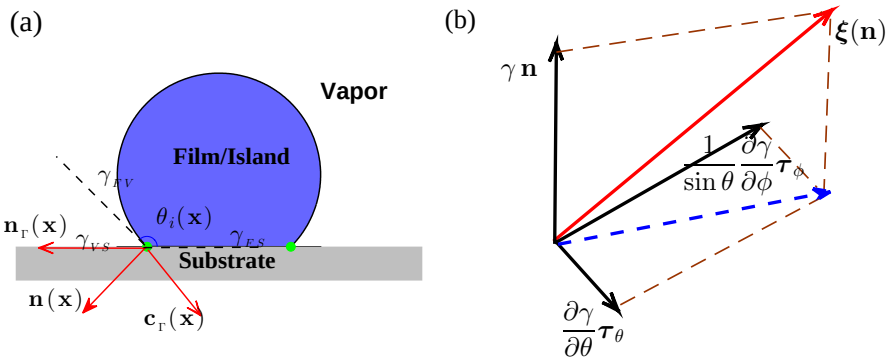

FIG. 3.1. *(a) The cross-section profile in configuration of the vectors along the contact line Γ. (b) The three components of the Cahn-Hoffman $\boldsymbol{\xi}$-vector.*

Eq. (3.4b) can be regarded as the Young equation for anisotropic surface energy $\gamma(\mathbf{n})$ in 3D. For isotropic surface energy, i.e., $\gamma(\mathbf{n}) \equiv 1$ (scaled by a constant γ_0), we have $\boldsymbol{\xi} = \mathbf{n}$ and $\mathbf{c}_\Gamma^\gamma = \mathbf{c}_\Gamma$. By simple calculations, Eq. (3.4a) will be reduced to the condition of constant mean curvature. Denote Γ_e as the boundary of S_e, for arbitrary $\mathbf{x} \in \Gamma_e$, let $\theta(\mathbf{x})$ represent the corresponding contact angle at boundary point $\mathbf{x}$. Then Eq. (3.4b) will reduce to

$$\cos\theta(\mathbf{x}) = \sigma, \quad \forall \mathbf{x} \in \Gamma_e, \tag{3.5}$$

where the material constant $\sigma := \frac{\gamma_{VS} - \gamma_{FS}}{\gamma_0}$, and it is the well-known isotropic Young equation [60]. For the anisotropic case, we can write the surface energy density in terms of the spherical coordinate, i.e., $\gamma_{FV} = \gamma(\theta, \phi)$ (scaled by a constant γ_0).

Therefore, the Cahn-Hoffman $\boldsymbol{\xi}$-vector can be decomposed into the following three components

$$\boldsymbol{\xi}(\mathbf{n}) = \nabla\hat{\gamma}(\mathbf{n}) = \gamma(\theta,\phi)\mathbf{n} + \frac{\partial\gamma(\theta,\phi)}{\partial\theta}\boldsymbol{\tau}_{\theta} + \frac{1}{\sin\theta}\frac{\partial\gamma(\theta,\phi)}{\partial\phi}\boldsymbol{\tau}_{\phi}, \tag{3.6}$$

where in these expressions,

$$\mathbf{n} = (\sin\theta\cos\phi, \sin\theta\sin\phi, \cos\theta)^T, \tag{3.7a}$$

$$\boldsymbol{\tau}_{\theta} = (\cos\theta\cos\phi, \cos\theta\sin\phi, -\sin\theta)^T, \tag{3.7b}$$

$$\boldsymbol{\tau}_{\phi} = (-\sin\phi, \cos\phi, 0)^T. \tag{3.7c}$$

Therefore, we obtain that the following expressions hold

$$\boldsymbol{\xi}\cdot\mathbf{n} = \gamma(\theta,\phi), \qquad \mathbf{c}_{\Gamma}\cdot\mathbf{n}_{\Gamma} = \cos\theta(\mathbf{x}). \tag{3.8a}$$

$$\boldsymbol{\xi}\cdot\mathbf{c}_{\Gamma} = \frac{\partial\gamma(\theta,\phi)}{\partial\theta}, \qquad \mathbf{n}\cdot\mathbf{n}_{\Gamma} = \sin\theta(\mathbf{x}). \tag{3.8b}$$

Thus we can rewrite Eq. (3.4b) as

$$\gamma(\theta,\phi)\cos\theta(\mathbf{x}) - \frac{\partial\gamma(\theta,\phi)}{\partial\theta}\sin\theta(\mathbf{x}) - \sigma = 0, \quad \forall\mathbf{x}\in\Gamma_e, \tag{3.9}$$

which is consistent with the anisotropic Young equation discussed for the solid-state dewetting problem in 2D [5, 52].

If $\mathbf{X} := \mathbf{X}(\theta,\phi)$ represents the position vector of a surface (e.g., the equilibrium shape S_e for a given $\gamma(\theta,\phi)$), then we have $\nabla_{_S}\cdot\mathbf{X} = 2$ by using Definition 2.1. Therefore, we obtain that an equilibrium shape of the solid-state dewetting problem could have the similar shape with the $\boldsymbol{\xi}$-plot from (3.4a). Based on the Winterbottom construction [53] and recent work for the generalized Winterbottom construction [5], we can construct its analytical expression for the equilibrium shape. First, we define a domain of definition $U_{_\phi}$ for θ under a fixed value ϕ as

$$U_{_\phi} := \Big\{\theta\Big|\gamma(\theta,\phi)\cos\theta - \frac{\partial\gamma(\theta,\phi)}{\partial\theta}\sin\theta - \sigma \geq 0, \quad \theta\in[0,\pi]\Big\}, \tag{3.10}$$

where $\sigma = \frac{\gamma_{_{VS}}-\gamma_{_{FS}}}{\gamma_0}$. Based on Lemma 3.1, we can explicitly construct its equilibrium shape in the parametric formula as $S_e(\theta,\phi) := \mathbf{X}(\theta,\phi) = (x(\theta,\phi), y(\theta,\phi), z(\theta,\phi))^T$,

$$\begin{cases} x(\theta,\phi) = \lambda\big[\gamma(\theta,\phi)\sin\theta\cos\phi + \frac{\partial\gamma(\theta,\phi)}{\partial\theta}\cos\theta\cos\phi - \frac{1}{\sin\theta}\frac{\partial\gamma(\theta,\phi)}{\partial\phi}\sin\phi\big], \\ y(\theta,\phi) = \lambda\big[\gamma(\theta,\phi)\sin\theta\sin\phi + \frac{\partial\gamma(\theta,\phi)}{\partial\theta}\cos\theta\sin\phi + \frac{1}{\sin\theta}\frac{\partial\gamma(\theta,\phi)}{\partial\phi}\cos\phi\big], \\ z(\theta,\phi) = \lambda\big[\gamma(\theta,\phi)\cos\theta - \frac{\partial\gamma(\theta,\phi)}{\partial\theta}\sin\theta - \sigma\big], \end{cases} \tag{3.11}$$

where $\phi\in[0,2\pi]$, $\theta\in U_{_\phi}$, and λ is the scaling constant determined by the total volume $|\Omega|$ and γ_0.

Based on the formula (3.11), the equilibrium shape under different types of surface energy anisotropies, e.g., the cubic anisotropy and regularized "cusped" anisotropy defined in Eq. (1.4), can be easily constructed. Fig. 3.2(a)-(c) depicts the equilibrium shapes for isotropic surface energy with the material constant σ chosen as $\sigma = \cos(\pi/3), \cos(\pi/2), \cos(3\pi/4)$, respectively. It clearly demonstrates the effect

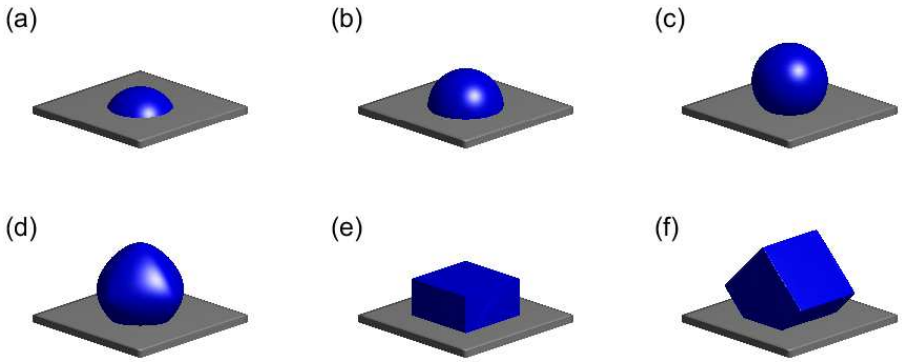

FIG. 3.2. *The equilibrium shape defined by Eq.* (3.11)*, where (a)-(c) is for isotropic surface energy, i.e.,* $\gamma(\mathbf{n}) \equiv 1$*, but with different material constants* $\sigma = \cos(\pi/3), \cos(\pi/2), \cos(3\pi/4)$*, respectively; (d)* $\gamma(\mathbf{n}) = 1 + 0.2(n_1^4 + n_2^4 + n_3^4)$*,* $\sigma = \cos(3\pi/4)$*; (e) The surface energy density is given by Eq.* (1.4)*, where* $\sigma = \cos(3\pi/4)$*,* $\varepsilon = 0.01$ *; (f) The surface energy density is given by* $\gamma(\boldsymbol{M}_x(\pi/4)\mathbf{n})$ *where* $\gamma(\mathbf{n})$ *is defined by Eq.* (1.4) *and* $\boldsymbol{M}_x(\pi/4)$ *represents the rotation for a matrix by an angle* $\pi/4$ *about the x-axis in 3D, using the right-hand rule, where* $\sigma = \cos(3\pi/4)$*,* $\varepsilon = 0.01$*.*

of the material constant σ on the equilibrium shape by influencing the equilibrium contact angle via (3.5). Moreover, we also present equilibrium shapes for the cubic anisotropic surface energy, i.e., $\gamma(\mathbf{n}) = 1+a(n_1^4+n_2^4+n_3^4)$ and regularized "cusped" surface energy defined in Eq. (1.4) with $\sigma = \cos(3\pi/4)$ in Fig. 3.2(d)-(e). The anisotropy for Fig. 3.2(f) is chosen by an anti-clockwise rotation along the x-axis by 45 degrees under the right-hand rule for the "cusped" surface energy. We can observe that this rotation results in a corresponding rotation of the equilibrium shape.

4. A sharp-interface model and its properties. In this section, we propose a kinetic sharp-interface model for simulating solid-state dewetting of thin films with anisotropic surface energies, and then we show that the proposed model satisfies the mass conservation and energy dissipation.

4.1. The model. Based on Eq. (2.35), we can define the first variation of the total interfacial energy functional with respect to the film/vapor interface S and its boundary curve (i.e., the contact line Γ) as

$$\frac{\delta W}{\delta S} = \nabla_{_S} \cdot \boldsymbol{\xi}, \qquad \frac{\delta W}{\delta \Gamma} = \mathbf{c}_{_\Gamma}^{\gamma} \cdot \mathbf{n}_{_\Gamma} + \gamma_{_{FS}} - \gamma_{_{VS}}. \tag{4.1}$$

From the Gibbs-Thomson relation [37, 50], the chemical potential can be defined as

$$\mu = \Omega_0 \frac{\delta W}{\delta S} = \Omega_0 \nabla_{_S} \cdot \boldsymbol{\xi}, \tag{4.2}$$

with Ω_0 representing the atomic volume. The normal velocity of the moving interface is controlled by surface diffusion [8, 37, 52, 25], and it can be defined as follows by Fick's laws of diffusion[4]

$$\mathbf{J} = -\frac{D_s \nu}{k_B\, T_e} \nabla_{_S}\, \mu, \qquad v_n = -\Omega_0 (\nabla_{_S} \cdot \mathbf{J}) = \frac{D_s \nu \Omega_0}{k_B\, T_e} \nabla_{_S}^2 \mu. \tag{4.3}$$

In these expressions, $\mathbf{J}$ is the mass flux of atoms, D_s is the surface diffusivity, $k_B\, T_e$ is the thermal energy, ν is the number of diffusing atoms per unit area, $\nabla_{_S}$ is the

surface gradient. In addition to the surface diffusion which controlled the motion of the moving interface, we still need the boundary condition for the moving contact line. Following the idea for simulating solid-state dewetting in 2D [52, 25], we assume that the normal velocity of the contact line Γ is simply given by the energy gradient flow, which is determined by the time-dependent Ginzburg-Landau kinetic equations, i.e.,

$$v_{n_\Gamma} = -\eta \frac{\delta W}{\delta \Gamma} = -\eta[\mathbf{c}_\Gamma^\gamma \cdot \mathbf{n}_\Gamma + \gamma_{FS} - \gamma_{VS}], \tag{4.4}$$

with $0 < \eta < \infty$ denoting the contact line mobility, which can be thought of as a reciprocal of a constant friction coefficient. For the physical explanation behind this approach, please refer to the recent paper [52].

We choose the characteristic length scale and characteristic surface energy scale as h_0 and γ_0, respectively, the time scale as $\frac{h_0^4}{B\gamma_0}$ with $B = \frac{D_s \nu \Omega_0^2}{k_B T_e}$, and the contact line mobility is scaled by $\frac{B}{h_0^3}$. Let $\mathbf{X}(\cdot, t) = (x(\cdot, t), y(\cdot, t), z(\cdot, t))^T$ be a local parameterization of the moving film/vapor interface S, then we can obtain a dimensionless kinetic sharp-interface model for solid-state dewetting of thin film via the following Cahn-Hoffman $\boldsymbol{\xi}$-vector formulation as

$$\partial_t \mathbf{X} = \Delta_S \mu \, \mathbf{n}, \qquad t > 0, \tag{4.5}$$

$$\mu = \nabla_S \cdot \boldsymbol{\xi}, \qquad \boldsymbol{\xi}(\mathbf{n}) = \nabla \hat{\gamma}(\mathbf{p})\Big|_{\mathbf{p}=\mathbf{n}}, \tag{4.6}$$

where t is the time, $\mathbf{n}$ is the unit outer normal vector of S, and $\boldsymbol{\xi} := \boldsymbol{\xi}(\mathbf{n})$ is the Cahn-Hoffman vector (scaled by γ_0). Here, for simplicity, we still use the same notations for all the dimensionless variables.

Let $\mathbf{X}_\Gamma(\cdot, t) = (x_\Gamma(\cdot, t), y_\Gamma(\cdot, t), z_\Gamma(\cdot, t))^T$ represents a parameterization of the moving contact line $\Gamma(t)$. The initial condition is given as S_0 with boundary Γ_0 such that

$$S_0 := \mathbf{X}(\cdot, 0) = (x_0, y_0, z_0), \quad \Gamma_0 := \mathbf{X}(\cdot, 0)\Big|_\Gamma. \tag{4.7}$$

The above governing equations are subject to the following boundary conditions:

(i) contact line condition

$$z_\Gamma(\cdot, t) = 0, \quad t \geq 0; \tag{4.8}$$

(ii) relaxed contact angle condition

$$\partial_t \mathbf{X}_\Gamma = -\eta\Big(\mathbf{c}_\Gamma^\gamma \cdot \mathbf{n}_\Gamma - \sigma\Big)\mathbf{n}_\Gamma, \qquad t \geq 0; \tag{4.9}$$

(iii) zero-mass flux condition

$$\Big(\mathbf{c}_\Gamma \cdot \nabla_S \, \mu\Big)\Big|_\Gamma = 0, \qquad t \geq 0; \tag{4.10}$$

where η represents a (dimensionless) contact line mobility, $\mathbf{c}_\Gamma^\gamma$ is the anisotropic co-normal vector which is defined as $\mathbf{c}_\Gamma^\gamma := (\boldsymbol{\xi} \cdot \mathbf{n})\, \mathbf{c}_\Gamma - (\boldsymbol{\xi} \cdot \mathbf{c}_\Gamma)\, \mathbf{n}$, $\mathbf{c}_\Gamma$ represents the co-normal vector, and $\mathbf{n}_\Gamma = (n_{\Gamma,1}, n_{\Gamma,2}, \ 0)^T$ is the outer unit normal vector of Γ on the substrate (cf. Fig. 2.1), and $\sigma = \frac{\gamma_{VS} - \gamma_{FS}}{\gamma_0}$ is a (dimensionless) material constant.

Remark 4.1. *The contact line condition in Eq.* (4.8) *ensures that the contact line must move along the substrate plane. Because the contact line* Γ *lies on the*

substrate (i.e., Oxy plane), the third component of $\mathbf{n}_\Gamma$ *is always zero, i.e.,* $n_{\Gamma,3} = 0$. *As long as the initial condition satisfies* $z_\Gamma(\cdot, 0) = 0$, *it can automatically satisfy the boundary condition (i)* $z_\Gamma(\cdot, t) = 0, \forall\, t > 0$ *by using the boundary condition (ii). The last boundary condition (iii) ensures that the total volume/mass of the thin film is conserved during the evolution, i.e., no-mass flux at the moving contact line.*

4.2. Mass conservation and energy dissipation. In the following, we will rigorously prove that the proposed sharp-interface model satisfies the mass conservation and the total free energy dissipation during the evolution.

PROPOSITION 4.1. *Assume that* $\mathbf{X}(\cdot, t)$ *is the solution of the sharp-interface model, i.e., Eqs.* (4.5)-(4.6) *with boundary conditions* (4.8)-(4.10), *and denote* $S(t) := \mathbf{X}(\cdot, t)$ *as the moving film/vapor interface. Then, the total volume (or mass) of the thin film, labeled as* $|\Omega(t)|$, *is conserved, i.e.,*

$$|\Omega(t)| \equiv |\Omega(0)|, \qquad t \geq 0. \tag{4.11}$$

Furthermore, the (dimensionless) total interfacial free energy of the system is non-increasing during the evolution, i.e.,

$$W(t) \leq W(t_1) \leq W(0) = \int_{S(0)} \gamma(\mathbf{n})\, dS - \sigma A(\Gamma(0)), \qquad t \geq t_1 \geq 0. \tag{4.12}$$

Proof. By making use of the first variation (2.21) and simply choosing the integrand $\psi(\mathbf{x}) \equiv 1, \forall\, \mathbf{x} \in \Omega$, and using the governing equation (4.5), we can calculate the time derivative of the total volume as (noting that $\mathbf{V}_0 = \partial_t \mathbf{X}$)

$$\frac{d}{dt}|\Omega(t)| = \int_{S(t)} \partial_t \mathbf{X} \cdot \mathbf{n}\, dS = \int_{S(t)} \Delta_{\scriptscriptstyle S} \mu\, dS = 0, \qquad t \geq 0, \tag{4.13}$$

where the last equality comes from the integration by parts and the zero-mass flux condition (4.10), and it indicates that the total volume/mass is conserved.

To obtain the time derivative of the (dimensionless) total free energy, by making use of Theorem 2.1 and Eq. (2.45), but replacing the perturbation variable ϵ with the time variable t, we can immediately obtain

$$\frac{d}{dt}W(t) = \int_{S(t)} (\nabla_{\scriptscriptstyle S} \cdot \boldsymbol{\xi})\, (\partial_t \mathbf{X} \cdot \mathbf{n})\, dS + \int_{\Gamma(t)} (\mathbf{c}_\Gamma^\gamma \cdot \mathbf{n}_\Gamma - \sigma)\, (\partial_t \mathbf{X}_\Gamma \cdot \mathbf{n}_\Gamma)\, d\Gamma.$$

By substituting the governing equations and the relaxed contact angle boundary condition, i.e.,

$$\mu = \nabla_{\scriptscriptstyle S} \cdot \boldsymbol{\xi}, \quad \Delta_{\scriptscriptstyle S} \mu = \partial_t \mathbf{X} \cdot \mathbf{n}, \quad \partial_t \mathbf{X}_\Gamma \cdot \mathbf{n}_\Gamma = -\eta(\mathbf{c}_\Gamma^\gamma \cdot \mathbf{n}_\Gamma - \sigma), \tag{4.14}$$

into the above equation and integrating by parts, we obtain

$$\begin{aligned} \frac{d}{dt}W(t) &= \int_{S(t)} \mu\, \Delta_S \mu\, dS - \eta \int_{\Gamma(t)} (\mathbf{c}_\Gamma^\gamma \cdot \mathbf{n}_\Gamma - \sigma)^2\, d\Gamma \\ &= -\int_{S(t)} |\nabla_{\scriptscriptstyle S} \mu|^2\, dS - \eta \int_{\Gamma(t)} (\mathbf{c}_\Gamma^\gamma \cdot \mathbf{n}_\Gamma - \sigma)^2\, d\Gamma \leq 0, \qquad t \geq 0, \end{aligned} \tag{4.15}$$

where the constant $\eta > 0$. The last inequality immediately implies the energy dissipation. ∎

REMARK 4.2. *In the above proof, we need to calculate the time derivatives of the total volume and the total free energy. These two derivatives can be easily obtained by making use of the speed method and the first variation presented in Section 2. In Section 2, we consider any type of smooth perturbations. In fact, a family of evolving interface surfaces* $\{S(t)\}_{t\geq 0}$ *can be also thought of as a type of perturbations, only by replacing the perturbation variable* ϵ *with the time variable* t*. Therefore, the time derivatives can be directly obtained by using the first variation of the total volume functional and the total free energy functional.*

5. Numerical results. In this section, we perform numerical simulations for solid-state dewetting in 3D to investigate the morphological evolution of thin films in various cases. We implement the parametric finite element method (PFEM) for solving the proposed sharp-interface model [6, 7].

5.1. Equilibrium convergence. We have presented a mathematical description of the equilibrium shape based in Section 3. Here, we present some numerical convergence to equilibrium shapes by solving the proposed kinetic sharp-interface model.

From the relaxed contact angle boundary condition (4.9), which describes the migration of the contact line, we know that the contact line mobility η precisely controls the relaxation rate of the contact angle towards its equilibrium state. The large η will accelerate the relaxation process [52]. Therefore, we numerically investigate the effect of η on the evolution of the dynamic contact angles. The evolution surfaces $\{S(t_m)\}_{m=1}^{M}$ are discretized by polygonal surfaces such that $S^m = \bigcup_{j=1}^{N} \bar{D}_j^m$, , where $\{D_j^m\}_{j=1}^{N}$ are mutually disjoint triangle surfaces, and the polygonal surface S^m has K vertices given as $\{\mathbf{q}_k^m\}_{k=1}^{K}$. The boundary of the polygonal surface S^m given by polygonal $\Gamma^m = \bigcup_{j=1}^{N_c} \bar{h}_j^m$, where $\{h_j^m\}_{j=1}^{N_c}$ are line segments of the curve ordered in counter-clockwise direction when viewing from the top. We define the following mean contact angles as the indicator,

$$\bar{\theta}^m = \frac{1}{N_c} \sum_{j=1}^{N_c} \arccos(\mathbf{c}_{\Gamma^m,j} \cdot \mathbf{n}_{\Gamma^m,j}), \tag{5.1}$$

where $\mathbf{c}_{\Gamma^m,j}$ and $\mathbf{n}_{\Gamma^m,j}$ are unit vector defined on line segment h_j. Fig. 5.1 shows the temporal evolution of $\bar{\theta}^m$ and the normalized energy $W(t)/W(0)$ under different choices of the contact line mobility η. The initial thin film is chosen as a unit cube. From the figure, we can observe that the larger mobility will accelerate the process of relaxation such that the contact angles evolve faster towards its equilibrium contact angle $3\pi/4$. Similarly, as shown in Fig. 5.1(b), the energy decays faster for larger mobility, but finally the equilibrium contact angle converges to the same value. It indicates that the equilibrium contact angles as well as the equilibrium shape are independent of the choice of the contact line mobility η. In the following numerical simulations, the contact line mobility is chosen to be very large, e.g.,$\eta = 100$. This choice of η will result in a very quick convergence to the equilibrium contact angle (defined by Eq. (3.4b)). The detailed investigation of the influence of the parameter on the solid-state dewetting evolution process and equilibrium shapes has been discussed in [52].

We next show a convergence result between the numerical equilibrium shape by solving the proposed sharp-interface model and its theoretical equilibrium shape. Fig. 5.2 shows the convergence results of the equilibrium shapes under different mesh

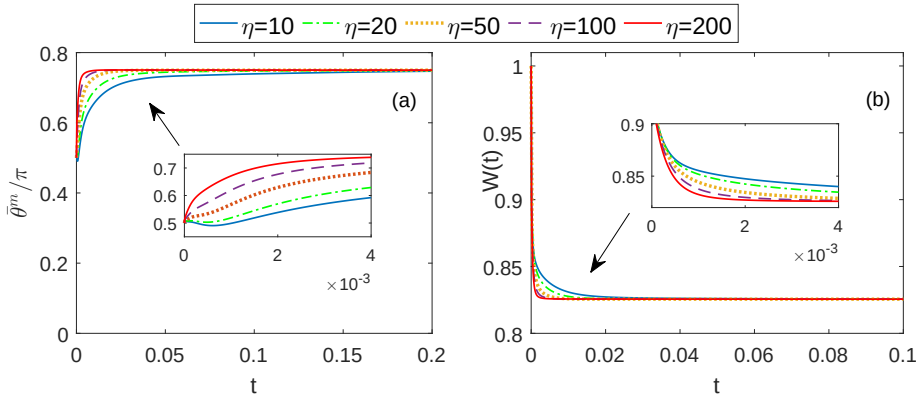

FIG. 5.1. *(a) The temporal evolution of contact angle $\bar{\theta}^m$ defined in Eq. (5.1); (b) the temporal evolution of the normalized energy $W(t)/W(0)$ for different choices of mobility, where the initial shape of the thin film with isotropic surface energy is chosen as a unit cube, and the computational parameters are chosen as $\sigma = \cos(3\pi/4)$.*

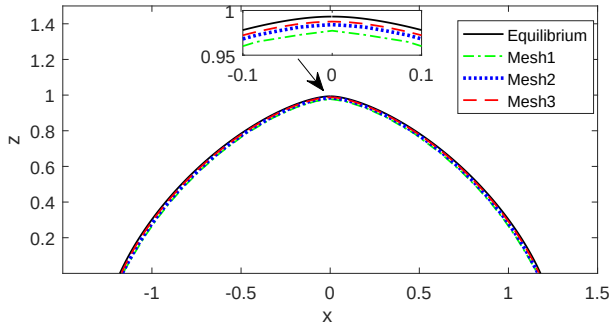

FIG. 5.2. *Comparison of the cross-section profiles in x-direction of the numerical equilibrium shapes under different meshes with its theoretical equilibrium shape, where the initial shape is chosen as a $(1, 2, 1)$ cuboid, the surface energy $\gamma(\mathbf{n}) = 1 + 0.25(n_1^4 + n_2^4 + n_3^4)$, and $\sigma = \cos(15\pi/36)$*

sizes, where $\sigma = \cos\frac{15\pi}{36}$, $\gamma(\mathbf{n}) = 1+0.25(n_1^4+n_2^4+n_3^4)$. The initial shape is chosen as a $(1, 2, 1)$ cuboid with different meshes, which are given by a set of small isosceles right triangles. If we define the mesh size indicator h as the length of the hypotenuse of the isosceles right triangle, then Mesh 1 represents the initial mesh with $h = h_0 = 0.125$, and the time step is chosen as $\tau = \tau_0 = 0.00125$ for numerical computation. Meanwhile, the time step for Mesh 2 ($h = \frac{h_0}{2}$) and Mesh 3 ($h = \frac{h_0}{4}$) are chosen as $\tau = \frac{\tau_0}{4}$ and $\tau = \frac{\tau_0}{16}$, respectively. For a better comparison, we plot the cross-section profiles along the x-direction for the numerical equilibrium shapes and the theoretical equilibrium shape. As shown in Fig. 5.2, we can clearly observe that as the computational mesh size gradually decreases, the numerical equilibrium shapes uniformly converge to the theoretical equilibrium shape (constructed by Eq. (3.11)).

5.2. Morphological evolution. We firstly focus on the case for isotropic surface energy, i.e., $\gamma(\mathbf{n}) \equiv 1$. We start with numerical examples for an initially, short cuboid island with $(2, 2, 1)$ representing its length, width and height, respectively (as

shown in Fig. 5.3(a)). The computational parameter is chosen as $\sigma = \cos\frac{5\pi}{6}$. As can be seen in Fig. 5.3, we show several snapshots of the morphology evolution for the short cuboid towards its equilibrium shape. As time evolves, the initial sharp corners and edges on the island become smooth in a very short time (Fig. 5.3(b)), and finally the thin film form a spherical shape as its equilibrium shape (Fig. 5.3(f)).

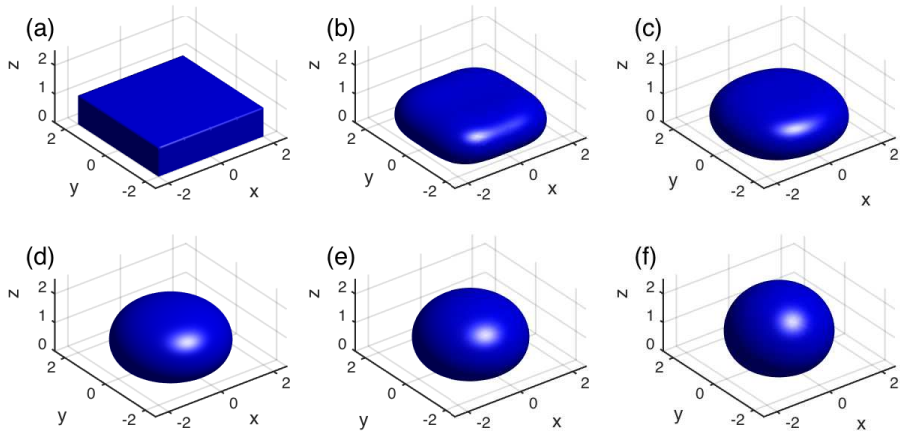

FIG. 5.3. *Several snapshots during the evolution of an initially, cuboid island film with isotropic surface energy towards its equilibrium shape: (a) $t = 0.0$; (b) $t = 0.1$; (c) $t = 0.2$; (d) $t = 0.5$; (e) $t = 0.7$; (f) $t = 1.40$, where the initial shape of the thin film is chosen as a $(2, 2, 1)$ cuboid, and the material constant is chosen as $\sigma = \cos(5\pi/6)$.*

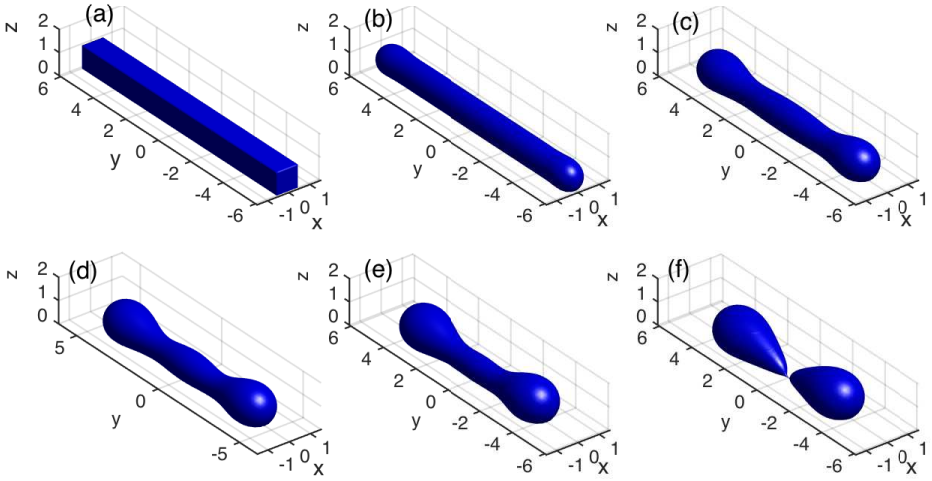

FIG. 5.4. *Several snapshots during the evolution of an initial, cuboid island film with isotropic surface energy until its pinch-off time: (a) $t = 0$; (b) $t = 0.01$; (c) $t = 0.30$; (d) $t = 0.50$; (e) $t = 0.80$; (f) $t = 1.03$, where the initial shape is chosen as a $(1, 12, 1)$ cuboid, and the material constant $\sigma = \cos(3\pi/4)$.*

Short cuboid island films tend to form a single island as its equilibrium shape with the spherical shape minimizing the total free energy (i.e., the minimal surface

area). However, the morphological evolution for long cuboid islands could be quite different during the evolution. Due to the Plateau-Rayleigh instability [44, 35], long cuboid islands will break up into a number of small isolated particles on the substrate before they are able to form the single spherical shape as its equilibrium. In order to investigate this phenomenon, we start the simulation by fixing the same material constant as $\sigma = \cos(3\pi/4)$, and choosing the initial thin film as a long cuboid with $(1, 12, 1)$. For isotropic case, as can be seen in Fig. 5.4, the island quickly evolves into a cylinder-like shape during the evolution, and then exhibits variations of the radius, and finally breaks up into two small isolated islands on the substrate. Under cubic anisotropic surface energies, long cuboid islands exhibit similar pinch-off phenomenon to the isotropic surface energy case. We test the numerical example for an initially cuboid island with the same material constant and initial island, as shown Fig. 5.5. From the figure, we observe that it finally forms three small isolated islands, while the island initially with the same shapes only form two isolated islands in the isotropic surface energy case. This indicates that in the cubic anisotropic surface energy, the solid island tends to dewet more easily than in the isotropic surface energy.

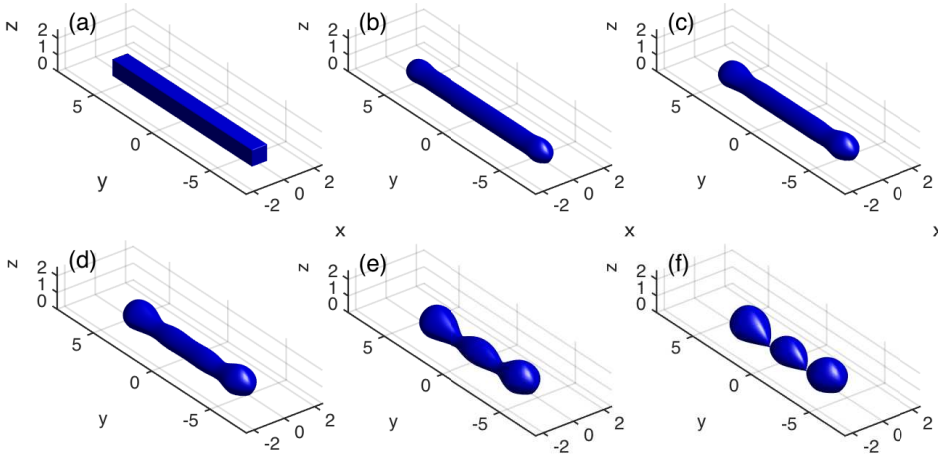

FIG. 5.5. *Several snapshots during the evolution of an initial, cuboid island film with anisotropic surface energy until its pinch-off time: (a) $t = 0$; (b) $t = 0.020$; (c) $t = 0.10$; (d) $t = 0.24$; (e) $t = 0.54$; (f) $t = 0.695$, where the initial shape is chosen as a $(1, 12, 1)$ cuboid, the material constant $\sigma = \cos(3\pi/4)$, and the anisotropic surface energy is chosen as the cubic type, i.e., $\gamma(\mathbf{n}) = 1 + a(n_1^4 + n_2^4 + n_3^4)$ with $a = 0.25$.*

We next examine the morphological evolutions of square island films with (m, m, h). We start by simulating the evolution of an initial, short square island with $(3.2, 3.2, 0.1)$, and the material constant is chosen as $\sigma = \cos\frac{5\pi}{6}$. As can be seen in Fig. 5.6, the four corners of the square island retract much more slowly than the middle points of the four edges at the beginning, thus resulting in a near cross shape for the island film (see Fig. 5.6(d)). This phenomenon of corner accumulation has also been observed in the experiments [51, 57, 59] or numerical simulations by the phase-field approach [23, 38]. These corners at last catch up with the edges and the contact line moves towards a circular shape in order to form a spherical shape as its equilibrium. Meanwhile, we can also observe that a valley forms at the center during the evolution, but finally disappear. However, if we enlarge the square size but fix the thickness of the initial thin film, the formed valley will become deep and finally touch the substrate, and

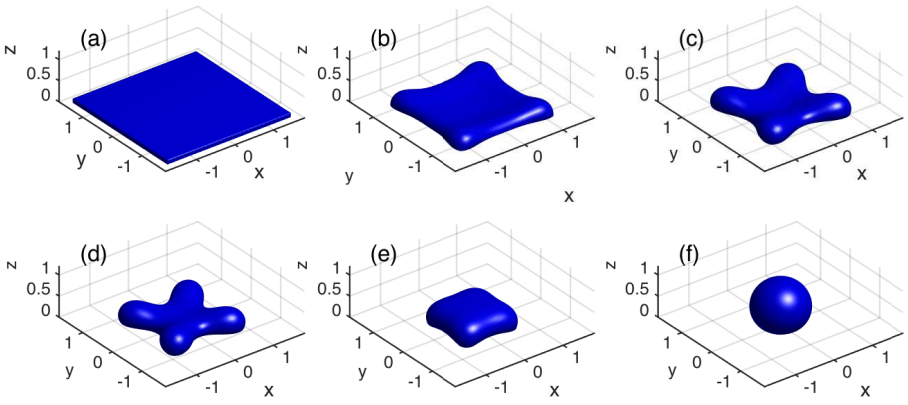

FIG. 5.6. *Several snapshots during the evolution of an initial, cuboid island film with isotropic surface energy towards its equilibrium shape: (a)* $t = 0$*; (b)* $t = 0.004$*; (c)* $t = 0.008$*; (d)* $t = 0.0120$*; (e)* $t = 0.020$*; (f)* $t = 0.080$*, where the initial shape is chosen as a* $(3.2, 3.2, 0.1)$ *cuboid, and the material constant* $\sigma = \cos(5\pi/6)$.

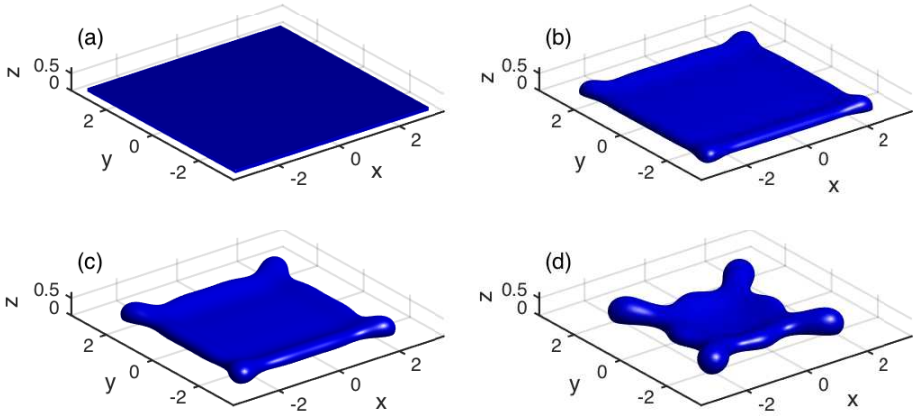

FIG. 5.7. *Several snapshots during the evolution of an initial, cuboid island film with isotropic surface energy until its pinch-off time: (a)* $t = 0$*; (b)* $t = 0.005$*; (c)* $t = 0.010$*; (d)* $t = 0.031$*, where the initial shape is chosen as a* $(6.4, 6.4, 0.1)$ *cuboid, and the material constant* $\sigma = \cos(5\pi/6)$.

produce a hole in the centre of the island, as shown in Fig. 5.7. We stop the numerical simulations at the time when there exists at least one mesh point which touches the substrate. For a better illustration, we also show the corresponding cross-section profiles of the thin film during the evolution in Fig. 5.8.

6. Conclusions. We proposed a sharp-interface approach for simulating solid-state dewetting of thin films in three dimensions (3D), and this approach can handle with the effect of the surface energy anisotropy. Based on the Cahn-Hoffman $\boldsymbol{\xi}$-vector formulation and the speed method, we derived rigorously the first variation of the total free energy functional of the solid-state dewetting problem. From the first variation, necessary conditions for the equilibrium shape of solid-state dewetting were rigorously given in mathematics. Furthermore, a kinetic sharp-interface model was also proposed

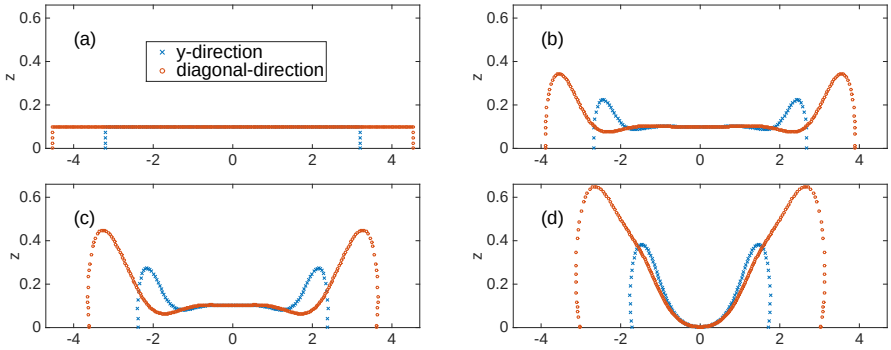

FIG. 5.8. *The cross-section profile of the thin film along its y-direction and diagonal direction for the example shown in Fig. 5.7: (a) $t = 0$; (b) $t = 0.005$; (c) $t = 0.010$; (d) $t = 0.031$.*

for simulating the solid-state dewetting of thin films in 3D. The governing equations described the interface evolution which is controlled by surface diffusion and contact line migration. A lot of numerical examples were performed for solving the model, and numerical results reproduced the complex features in the solid thin film dewetting observed in experiments, such as hole formation, corner accumulation, pinch-off and Rayleigh instability.

REFERENCES

[1] D. AMRAM, L. KLINGER, AND E. RABKIN, *Anisotropic hole growth during solid-state dewetting of single-crystal Au–Fe thin films*, Acta Mater., 60 (2012), pp. 3047–3056.

[2] L. ARMELAO, D. BARRECA, G. BOTTARO, A. GASPAROTTO, S. GROSS, C. MARAGNO, AND E. TONDELLO, *Recent trends on nanocomposites based on Cu, Ag and Au clusters: A closer look*, Coord. Chem. Rev., 250 (2006), pp. 1294–1314.

[3] R. BACKOFEN, S. M. WISE, M. SALVALAGLIO, AND A. VOIGT, *Convexity splitting in a phase field model for surface diffusion*, arXiv:1710.09675, (2017).

[4] R. W. BALLUFFI, S. ALLEN, AND W. C. CARTER, *Kinetics of materials*, John Wiley & Sons, 2005.

[5] W. BAO, W. JIANG, D. J. SROLOVITZ, AND Y. WANG, *Stable equilibria of anisotropic particles on substrates: a generalized winterbottom construction*, SIAM J. Appl. Math, 77 (2017), pp. 2093–2118.

[6] W. BAO, W. JIANG, Y. WANG, AND Q. ZHAO, *A parametric finite element method for solid-state dewetting problems with anisotropic surface energies*, J. Comput. Phys., 330 (2017), pp. 380–400.

[7] W. BAO, W. JIANG, AND Q. ZHAO, *A parametric finite element method for solid-state dewetting problems in three dimensions*, in preparation, (2018).

[8] J. CAHN AND D. HOFFMAN, *A vector thermodynamics for anisotropic surfaces: I. curved and faceted surfaces*, Acta Metall., 22 (1974), pp. 1205–1214.

[9] J. W. CAHN AND C. A. HANDWERKER, *Equilibrium geometries of anisotropic surfaces and interfaces*, Mater. Sci. Eng: A, 162 (1993), pp. 83–95.

[10] W. C. CARTER, A. R. ROOSEN, J. W. CAHN, AND J. E. TAYLOR, *Shape evolution by surface diffusion and surface attachment limited kinetics on completely faceted surfaces*, Acta Metall. Mater., 43 (1995), pp. 4309–4323.

[11] D. T. DANIELSON, D. K. SPARACIN, J. MICHEL, AND L. C. KIMERLING, *Surface-energy-driven dewetting theory of silicon-on-insulator agglomeration*, J. Appl. Phys., 100 (2006), p. 083507.

[12] K. DECKELNICK, G. DZIUK, AND C. M. ELLIOTT, *Computation of geometric partial differential equations and mean curvature flow*, Acta Numer., 14 (2005), pp. 139–232.

[13] G. DOĞAN AND R. H. NOCHETTO, *First variation of the general curvature-dependent surface energy*, ESAIM: M2AN, 46 (2012), pp. 59–79.

[14] E. Dornel, J. Barbe, F. De Crécy, G. Lacolle, and J. Eymery, *Surface diffusion dewetting of thin solid films: Numerical method and application to Si/SiO_2*, Phys. Rev. B, 73 (2006), p. 115427.
[15] M. Dufay and O. Pierre-Louis, *Anisotropy and coarsening in the instability of solid dewetting fronts*, Phys. Rev. Lett., 106 (2011), p. 105506.
[16] G. Dziuk and C. M. Elliott, *Finite element methods for surface PDEs*, Acta Numer., 22 (2013), pp. 289–396.
[17] M. Dziwnik, A. Münch, and B. Wagner, *Sharp interface limits of an anisotropic phase field model for solid-state dewetting*, IFAC-PapersOnLine, 48 (2015), pp. 394–395.
[18] Y. Fan, R. Nuryadi, Z. A. Burhanudin, and M. Tabe, *Thermal agglomeration of ultrathin silicon-on-insulator layers: Crystalline orientation dependence*, Jpn. J. Appl. Phys, 47 (2008), p. 1461.
[19] C. Herring, *The Physics of Powder Metallurgy, edited by W.E. Kingston*, McGraw-Hill, New York, 1951.
[20] A. Herz, A. Franz, F. Theska, M. Hentschel, T. Kups, D. Wang, and P. Schaaf, *Solid-state dewetting of single-and bilayer Au-W thin films: Unraveling the role of individual layer thickness, stacking sequence and oxidation on morphology evolution*, AIP Adv., 6 (2016), p. 035109.
[21] M. Hintermüller and W. Ring, *A second order shape optimization approach for image segmentation*, SIAM J. Appl. Math., 64 (2004), pp. 442–467.
[22] D. W. Hoffman and J. W. Cahn, *A vector thermodynamics for anisotropic surfaces: I. fundamentals and application to plane surface junctions*, Surface Science, 31 (1972), pp. 368–388.
[23] W. Jiang, W. Bao, C. V. Thompson, and D. J. Srolovitz, *Phase field approach for simulating solid-state dewetting problems*, Acta Mater., 60 (2012), pp. 5578–5592.
[24] W. Jiang, Y. Wang, D. J. Srolovitz, and W. Bao, *Solid-state dewetting on curved substrates*, Phys. Rev. Mater., 2 (2018), p. 113401.
[25] W. Jiang, Y. Wang, Q. Zhao, D. J. Srolovitz, and W. Bao, *Solid-state dewetting and island morphologies in strongly anisotropic materials*, Scripta Mater., 115 (2016), pp. 123–127.
[26] W. Jiang and Q. Zhao, *Sharp-interface approach for simulating solid-state dewetting in two dimensions: a Cahn-Hoffman $\boldsymbol{\xi}$-vector formulation*, Physica D, (2019).
[27] W. Jiang, Q. Zhao, T. Qian, D. J. Srolovitz, and W. Bao, *Application of Onsager's variational principle to the dynamics of a solid toroidal island on a substrate*, Acta Mater., 163 (2019), pp. 154–160.
[28] E. Jiran and C. Thompson, *Capillary instabilities in thin films*, J. Electron. Mater., 19 (1990), pp. 1153–1160.
[29] E. Jiran and C. Thompson, *Capillary instabilities in thin, continuous films*, Thin Solid Films, 208 (1992), pp. 23–28.
[30] W. Kan and H. Wong, *Fingering instability of a retracting solid film edge*, J. Appl. Phys., 97 (2005), p. 043515.
[31] G. H. Kim and C. V. Thompson, *Effect of surface energy anisotropy on Rayleigh-like solid-state dewetting and nanowire stability*, Acta Mater., 84 (2015), pp. 190–201.
[32] G. H. Kim, R. V. Zucker, J. Ye, W. C. Carter, and C. V. Thompson, *Quantitative analysis of anisotropic edge retraction by solid-state dewetting of thin single crystal films*, J. Appl. Phys., 113 (2013), p. 043512.
[33] O. Kovalenko, S. Szabó, L. Klinger, and E. Rabkin, *Solid state dewetting of polycrystalline Mo film on sapphire*, Acta Mater., 139 (2017), pp. 51–61.
[34] F. Leroy, F. Cheynis, Y. Almadori, S. Curiotto, M. Trautmann, J. Barbé, P. Müller, et al., *How to control solid state dewetting: A short review*, Surface Science Reports, 71 (2016), pp. 391–409.
[35] M. S. McCallum, P. W. Voorhees, M. J. Miksis, S. H. Davis, and H. Wong, *Capillary instabilities in solid thin films: Lines*, J. appl. phys, 79 (1996), pp. 7604–7611.
[36] J. Mizsei, *Activating technology of SnO_2 layers by metal particles from ultrathin metal films*, Sensors and Actuators B: Chemical, 16 (1993), pp. 328–333.
[37] W. W. Mullins, *Theory of thermal grooving*, J. Appl. Phys., 28 (1957), pp. 333–339.
[38] M. Naffouti, R. Backofen, M. Salvalaglio, T. Bottein, M. Lodari, A. Voigt, T. David, A. Benkouider, I. Fraj, L. Favre, et al., *Complex dewetting scenarios of ultrathin silicon films for large-scale nanoarchitectures*, Sci. Adv., 3 (2017), p. eaao1472.
[39] M. Naffouti, T. David, A. Benkouider, L. Favre, A. Delobbe, A. Ronda, I. Berbezier, and M. Abbarchi, *Templated solid-state dewetting of thin silicon films*, Small, 12 (2016), pp. 6115–6123.
[40] D. Peng, S. Osher, B. Merriman, and H.-K. Zhao, *The geometry of Wulff crystal shapes and its relations with Riemann problems*, Nonlinear Partial Differential Equations: Evanston,

IL, (1998), pp. 251–303.
[41] O. Pierre-Louis, A. Chame, and Y. Saito, *Dewetting of ultrathin solid films*, Phys. Rev. Lett., 103 (2009), p. 195501.
[42] E. Rabkin, D. Amram, and E. Alster, *Solid state dewetting and stress relaxation in a thin single crystalline Ni film on sapphire*, Acta Mater., 74 (2014), pp. 30–38.
[43] S. Randolph, J. Fowlkes, A. Melechko, K. Klein, H. Meyer III, M. Simpson, and P. Rack, *Controlling thin film structure for the dewetting of catalyst nanoparticle arrays for subsequent carbon nanofiber growth*, Nanotechnology, 18 (2007), p. 465304.
[44] L. Rayleigh, *On the instability of jets*, Proc. Lond. Math. Soc, 1 (1878), pp. 4–13.
[45] V. Schmidt, J. V. Wittemann, S. Senz, and U. Gösele, *Silicon nanowires: a review on aspects of their growth and their electrical properties*, Adv. Mater, 21 (2009), pp. 2681–2702.
[46] A. Shklyaev and A. Budazhapova, *Submicron-and micron-sized sige island formation on si (100) by dewetting*, Thin Solid Films, 642 (2017), pp. 345–351.
[47] J. Sokołowski and J. Zolesio, *Introduction to shape optimization: Shape sensitivity analysis. 1992*.
[48] D. J. Srolovitz and S. A. Safran, *Capillary instabilities in thin films: I. Energetics*, J. Appl. Phys., 60 (1986), pp. 247–254.
[49] D. J. Srolovitz and S. A. Safran, *Capillary instabilities in thin films: II. Kinetics*, J. Appl. Phys., 60 (1986), pp. 255–260.
[50] A. P. Sutton and R. W. Balluffi, *Interfaces in crystalline materials*, Clarendon Press, 1995.
[51] C. V. Thompson, *Solid-state dewetting of thin films*, Annu. Rev. Mater. Res., 42 (2012), pp. 399–434.
[52] Y. Wang, W. Jiang, W. Bao, and D. J. Srolovitz, *Sharp interface model for solid-state dewetting problems with weakly anisotropic surface energies*, Phys. Rev. B, 91 (2015), p. 045303.
[53] W. Winterbottom, *Equilibrium shape of a small particle in contact with a foreign substrate*, Acta Metall., 15 (1967), pp. 303–310.
[54] H. Wong, P. Voorhees, M. Miksis, and S. Davis, *Periodic mass shedding of a retracting solid film step*, Acta Mater., 48 (2000), pp. 1719–1728.
[55] G. Wulff, *Zur frage der geschwindigkeit des wachstums und der auflösung der krystallflächen*, Z. Kristallogr, 34 (1901), pp. 449–530.
[56] J. Ye and C. V. Thompson, *Mechanisms of complex morphological evolution during solid-state dewetting of single-crystal nickel thin films*, Appl. Phys. Lett., 97 (2010), p. 071904.
[57] J. Ye and C. V. Thompson, *Regular pattern formation through the retraction and pinch-off of edges during solid-state dewetting of patterned single crystal films*, Phys. Rev. B, 82 (2010), p. 193408.
[58] J. Ye and C. V. Thompson, *Anisotropic edge retraction and hole growth during solid-state dewetting of single crystal nickel thin films*, Acta Mater., 59 (2011), pp. 582–589.
[59] J. Ye and C. V. Thompson, *Templated solid-state dewetting to controllably produce complex patterns*, Adv. Mater., 23 (2011), pp. 1567–1571.
[60] T. Young, *An essay on the cohesion of fluids*, Philos. Trans. R. Soc. London, 95 (1805), pp. 65–87.
[61] R. V. Zucker, G. H. Kim, W. C. Carter, and C. V. Thompson, *A model for solid-state dewetting of a fully-faceted thin film*, Comptes Rendus Physique, 14 (2013), pp. 564–577.
[62] R. V. Zucker, G. H. Kim, J. Ye, W. C. Carter, and C. V. Thompson, *The mechanism of corner instabilities in single-crystal thin films during dewetting*, J. Appl. Phys., 119 (2016), p. 125306.